A momentum subspace method for the model-order reduction in nonlinear structural dynamics

Theory and experiments

Sinha, Kautuk; Singh, Niels K.; Abdalla, Mostafa M.; De Breuker, Roeland; Alijani, Farbod

DOI
10.1016/j.ijnonlinmec.2019.103314

Publication date
2020

Document Version
Accepted author manuscript

Published in
International Journal of Non-Linear Mechanics

A Momentum Subspace Method for the Model-order Reduction in Nonlinear Structural Dynamics : Theory and Experiments

Kautuk Sinha[a,*], Niels K. Singh[a], Mostafa M. Abdalla[b], Roeland De Breuker[a], Farbod Alijani[c]

[a]*Department of Aerospace Structures and Materials, Faculty of Aerospace Engineering, Delft University of Technology, Kluyverweg 1, 2629 HS, Delft, the Netherlands*
[b]*Zewail City of Science and Technology, Sheikh Zayed District, 12588, Giza, Egypt*
[c]*Department of Precision and Microsystems Engineering, Faculty of Mechanical, Maritime and Materials Engineering, Delft University of Technology, Mekelweg 2, 2628 CD, Delft, the Netherlands*

Abstract

The article proposes a method developed for model order reduction in a Finite Element (FE) framework that is capable of computing higher order stiffness tensors. In the method, a truncated third order asymptotic expansion is used for transformation of an FE model to a reduced system. The basis matrix in the formulation of the reduced-order model (ROM) is derived from linear mode shapes of the structure. The governing equations are derived using Hamilton's principle and the method is applied to geometrically nonlinear vibration problems to test its effectiveness. An initial validation of the numerical formulation is obtained by comparison of results from time domain nonlinear vibration analyses of a rectangular plate using Abaqus. Subsequently, a stiffened plate is modelled to test a more complex structure and a continuation algorithm is used in combination with the ROM to compute nonlinear frequency response curves. The validation of the stiffened plate has been performed through comparisons with the results of nonlinear vibration experiments. The experiments are conducted with Polytec Laser Doppler Vibrometer and PAK MK-II measurement systems for large amplitude vibrations to validate the nonlinear vibration analyses.

Keywords:
Model Order Reduction, Hamiltonian Mechanics, Finite Element Method, Nonlinear vibrations

1. Introduction

Thin-walled and flexible mechanical structures are often susceptible to large amplitude vibrations in operating conditions which activates geometric nonlinearity in the structural response. Nonlinear dynamic analyses of such structures using full-scale Finite Element (FE) models can require a high computational effort which further magnifies with the increase in complexity of the model and accuracy requirements. These analyses are becoming increasingly important in the early design stages of structures in industry. To overcome the drawback, model condensation and model reduction methods are highly advantageous.

A typically known model reduction method is the Modal Superposition method [1], in which a modal matrix is constructed by selecting eigenvectors corresponding to the lowest frequency natural model. The Ritz-Wilson Method [2] and Proper Orthogonal Decomposition [3, 4] are other well known reduction techniques. In the former, Ritz vectors are obtained with the advantage that they are less expensive to compute than natural modes, while in the latter snapshots of the time response are used to build a reduced basis. The Ritz-Wilson method was extended to nonlinear structural dynamics in [5]. Noor & Peters [6] presented a method to predict the nonlinear static response of structures by employing a Rayleigh-Ritz technique to approximate the governing FE equations by a reduced system. The basis vectors used herein are a nonlinear solution of the nodal displacement and path derivatives.

*Kautuk Sinha, Present Address: Institute of Aeroelasticity, German Aerospace Center, Bunsenstrasse 10, 37073, Germany
Email addresses: kautuk.sinha@dlr.de (Kautuk Sinha), nielssingh@outlook.com (Niels K. Singh), moabdall@zewailcity.edu.eg (Mostafa M. Abdalla), R.DeBreuker@tudelft.nl (Roeland De Breuker), F.Alijani@tudelft.nl (Farbod Alijani)

A significant consequence of the nonlinearity is frequency -amplitude dependency, i.e. a corresponding shift in the modal frequency with variation of vibration amplitude. The change in resonance frequency arises due to hardening or softening type nonlinearity which becomes more prominent with the increase in vibration amplitude [7]. Considerations for geometric nonlinearity in the dynamic analysis of thin walled structures have been recognized since the pioneering work of Chu & Herrmann [8] who obtained the backbone curve of a simply supported plate using perturbation methods. Eisley [9] derived the amplitude –frequency correlation of a plate using first order approximation in the Ritz method. Yamaki & Chiba [10] proposed a method using Harmonic balance approach with a third order Galerkin approximation. The validation of this study was performed by Yamaki et al. [11] by conducting experiments on a square plate with clamped boundary conditions. A Galerkin discretization with symplectic integration was used to obtain backbone curves of simply supported rectangular plates with different aspect ratios by Leung & Mao [12]. The study demonstrated symplectic integration as a numerical algorithm with negligibly small artificial damping in comparison to Runge-Kutta method. Nonlinear vibrations of isotropic and laminated plates using Hierarchial Finite element method was studied by Han & Petyt [13, 14]. Considerations of in-plane displacements in this formulation showed a significant variance in nonlinear dynamic response in comparison to the formulation neglecting in-plane displacements. The same was also shown by Alijani & Amabili [15] in studying large amplitude vibrations of laminated and sandwich plates using shear deformation theories for the numerical formulation. An initial assumption of solution was chosen to be a product of spatial and temporal component where the spatial part was expanded as Chebyshev polynomials. Furthermore, a reduced-order model was implemented by utilization of appropriately selected linear eigenmodes as shape functions. The governing equations were then solved using a continuation scheme. A ROM for angle-ply laminated cylindrical shells using vibration modes as the basis is presented by Amabili [16]. A method for retention of appropriate modes in the reduction procedure has also been presented which is valid for circular shells with uniform boundary conditions and any generic lamination sequence. A more extensive review of the literature on the nonlinear vibrations of plates and shells can be found in [17] and further in [18].

A family of ROMs with formulations based on enrichment of basis matrix by using higher order terms or modal derivatives (MD) along with vibration modes has seen prominent development in recent years. Idelsohn & Cardona [19] presented the use of modal derivatives along with tangent modes in the basis matrix used for the formulation of the reduced order model (ROM). The proposition is based on the premise that the tangent modes, being a function of displacements, can be expanded by using the Taylor series. While a linearization approximation is valid in the case of small displacements, the nonlinear effect is not captured for higher amplitudes. In [20], three approaches for formulating the basis matrix are presented and compared which include the use of only tangent modes, tangent modes in combination with modal derivatives and tangent modes in combination with the newly introduced and so termed static modes. Static modes are calculated as a steady state solution of the structure using Newton-Raphson approach. It is shown that adding modal derivatives in the ROM basis along with tangent modes significantly improves the accuracy of the nonlinear response. Addition of static modes is shown to have a similar improvement in the accuracy of the obtained results. However, no cumulative improvement could be seen through addition of both- modal derivatives and static modes. A perturbation method, based on the theory of initial post-buckling behaviour developed by Koiter [21] and extended to free vibrations in an analytical framework by Rehfield [22], was generalized to a finite element context by Tiso [23]. This method demonstrated how the enrichment of the basis with second order modes yields more accurate results compared to a full finite element analysis. A criterion is introduced in [24] which allows selection of the most important second order modes for the basis, prior to computing them. It is based on the convergence of the underlying linear dynamics problem. The proposed criterion looks at the spatial and spectral properties of the eigenspectrum and the applied load. The computation of nonlinear normal modes of geometrically nonlinear planar structures using a reduced-order model is presented in [25]. The FE model is reduced using a Galerkin projection and a basis is used consisting of linear vibration modes and modal derivatives.

However, as pointed out by Jain et al. [26], the basis rapidly increases in size with the complexity of the structure when modal derivatives are included and more vibration modes are required to capture the response accurately. This can be alleviated to some extent by incorporation of a modal derivative selection process, however, this is not robust for different load cases. The authors, therefore, propose a quadratic mapping for the displacement transformation to capture the effect of geometric non-linearity in their so called quadratic manifold approach. Vibration modes are utilized as coefficients for the linear term while modal derivatives are used as coefficients for the quadratic term in the nonlinear mapping. A generalization of the quadratic manifold approach has been presented by Rutzmoser et al. [27]

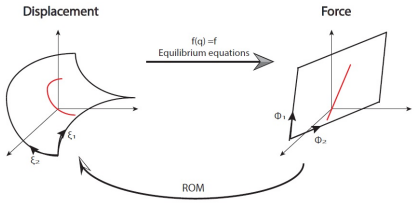

Figure 1: Mapping from the displacement space to the force space [28]

which enables utilization of arbitrary ROM bases. The basis is a derivative of the quadratic mapping used, therefore, resulting in displacement dependent mass, damping and stiffness tensors. The quadratic manifold approach shows that the use of quadratic mapping eliminates the shortcomings of using modal derivatives in the ROM basis when a linear mapping is used for displacement, with minimal loss in accuracy. The basis used in this method is a first derivative of the nonlinear displacement mapping and therefore, results in a configuration dependent mass and damping in the ROM.

In this paper a momentum subspace method is proposed to predict the dynamic response of geometrically nonlinear structures which is an extension of the Koiter-Newton approach [28, 29]. A nonlinear mapping of the displacement space is assumed with expansion in a Taylor series up to second order. The momentum, however, is assumed to be a linear combination of basis vectors, essentially used to define inertial force as a static component based on D'Alembert's principle. The use of displacements and momenta makes it convenient to employ the Hamiltonian formulation to describe the dynamics of the system. The method works in tandem with a FE formulation procedure which computes the higher order stiffness tensors for a high fidelity FE model. In the present case, up to cubic nonlinearity has been considered in the nonlinear restoring force function, therefore the method is compatible with FEM tools capable of computing quadratic and cubic stiffness tensors. The FEM formulation used in this study has been further elaborated in the subsequent sections. The ROM basis is presently derived only using linear vibration modes, however, the method offers the possibility to use any generic ROM basis.

2. Theory

2.1. Review of the Koiter-Newton Approach

The momentum sub-space method, as developed in this work, is an extension of the static reduction method, known as the Koiter-Newton approach given in [28]. The aim of this method was to find a new analytical approach to nonlinear structural problems in the presence of buckling. The method uses the asymptotic technique to replace the governing equations of a structure by a reduced system of equations.
Liang [28] states that the discretized equilibrium equations of a structure can be reduced to a set of nonlinear equations of the form:

$$\mathbf{f}(\mathbf{q}) = \lambda \mathbf{f}_{ex}, \tag{1}$$

where $\mathbf{f}$ is the internal force vector, $\mathbf{f}_{ex}$ is the external load vector, λ is the load parameter and $\mathbf{q}$ is the vector containing the degrees of freedom. As shown in Figure 1, Equation 1 defines a curve in the displacement space, referred to as the equilibrium path. This equation can be interpreted as a mapping from the displacement space to the force space, and the equilibrium path can be thought of as the pre-image of the line $\mathbf{f} = \lambda - \mathbf{f}_{ex}$ in the displacement space. In the Koiter-Newton approach a reduced-order model is constructed to approximate the equilibrium equations in the neighbourhood of a known equilibrium state which is referred to as ($\mathbf{q}_0$,λ_0). The vector $\mathbf{q}_0$ is the response of the structure at this equilibrium state, which is referred to as the nominal configuration and λ_0 is the load parameter. $\mathbf{q}$ is the unknown displacement vector near this nominal configuration resulting in:

$$\mathbf{q} = \mathbf{q}_0 \circ \mathbf{u}, \tag{2}$$

in which $\mathbf{u}$ describes the current configuration with respect to the nominal configuration and $\circ$ is the composition operator. The composition of displacements in $\mathbf{u}$ and $\mathbf{q}_0$ is an addition, however for beams and shells where finite rotations are taken into account, the composition operations depends on the parametrisation of rotations [30, 28].

The Koiter-Newton method is applicable to buckling sensitive structures. When buckling occurs, multiple secondary equilibrium branches that intersect with the primary path at buckling exist. Specific perturbation loads are selected that excite these secondary branches. This is achieved by a linear subspace of the force, containing the loading line. The subspace is defined as the span of predefined force vectors. This implies that it can be parametrised by the coordinates ϕ along the predefined force directions. The force subspace $\mathbf{f}$ is given as:

$$\mathbf{f} = \mathsf{F}\boldsymbol{\phi}, \tag{3}$$

in which F is the load matrix containing the sub-load vectors and the coordinates ϕ represent the amplitudes of these sub-loads. The pre-image of the force subspace in the displacement space is in general a nonlinear surface, as shown in Figure 1. It is a complex task to construct the pre-image of the force subspace. For this reason, an approximation of the nonlinear surface is found using a Taylor series expansion of the third order with respect to $\mathbf{u}$ as:

$$\mathcal{L}(\mathbf{u}) + Q(\mathbf{u},\mathbf{u}) + C(\mathbf{u},\mathbf{u},\mathbf{u}) = \mathsf{F}\boldsymbol{\phi}, \tag{4}$$

in which the symbols $\mathcal{L}$, Q and C are used to represent the linear, quadratic and cubic forms in the expansion. L, Q and C are their corresponding tensors, representing stiffness terms. For example, the quadratic operator $Q(\mathbf{u},\mathbf{u})$ can be read as $Q_{\alpha\beta\gamma}u_\beta u_\gamma$, where u_β and u_γ are components of the vector $\mathbf{u}$. $Q_{\alpha\beta\gamma}$ is the entry in the three-dimensional tensor Q. Note that the Einstein summation convention is applied. An approximate solution for Equation 4 is found in terms of a Taylor series expansion. This expansion defines the displacement subspace. This equilibrium surface is parametrised in terms of the generalised displacements vector $\boldsymbol{\xi}$. The expansion is performed up to third order and is given as:

$$\mathbf{u} = \mathbf{u}_\alpha\xi_\alpha + \mathbf{u}_{\alpha\beta}\xi_\alpha\xi_\beta + \mathbf{u}_{\alpha\beta\gamma}\xi_\alpha\xi_\beta\xi_\gamma, \tag{5}$$

in which $\mathbf{u}_\alpha$, $\mathbf{u}_{\alpha\beta}$, $\mathbf{u}_{\alpha\beta\gamma}$ are the first, second and third order displacement fields, respectively.

The equilibrium surface may be parametrised with an infinite number of choices for $\boldsymbol{\xi}$. This parametrisation is fixed by choosing the vector $\boldsymbol{\xi}$ to be work conjugate to the load amplitudes $\boldsymbol{\phi}$, as given by:

$$(\mathsf{F}\boldsymbol{\phi})^t\,\delta\mathbf{u} \equiv \boldsymbol{\phi}^t\delta\boldsymbol{\xi}. \tag{6}$$

To make this equation hold for any value of $\boldsymbol{\xi}$, the coefficients of the derivatives must satisfy the constraint equations, or orthogonality constraints given as:

$$\begin{cases} \mathbf{f}_\alpha^t\mathbf{u}_\beta = \delta_{\alpha\beta} & \text{(7a)} \\ \mathbf{f}_\alpha^t\mathbf{u}_{\beta\gamma} = 0 & \text{(7b)} \\ \mathbf{f}_\alpha^t\mathbf{u}_{\beta\gamma\delta} = 0, & \text{(7c)} \end{cases}$$

with $\delta_{\alpha\beta}$ being the Kronecker delta. In a similar fashion as the displacement expansion from Equation 5, the load amplitudes $\boldsymbol{\phi}$ are expanded as a function of $\boldsymbol{\xi}$. This represents the reduced-order model:

$$\boldsymbol{\phi} = \bar{\mathcal{L}}(\boldsymbol{\xi}) + \bar{Q}(\boldsymbol{\xi},\boldsymbol{\xi}) + \bar{C}(\boldsymbol{\xi},\boldsymbol{\xi},\boldsymbol{\xi}), \tag{8}$$

in which $\bar{\mathcal{L}}$, $\bar{Q}$ and $\bar{C}$ are linear, quadratic and cubic forms. $\bar{\mathsf{L}}$, $\bar{\mathsf{Q}}$ and $\bar{\mathsf{C}}$ are multiple dimensional tensors. To obtain the first and second order displacement fields, two sets of linear finite element systems need to be solved:

$$\begin{bmatrix} \mathsf{K}_t & -\mathsf{F} \\ -\mathsf{F}^t & 0 \end{bmatrix} \begin{Bmatrix} \mathbf{u}_\alpha \\ \bar{\mathbf{L}}_\alpha \end{Bmatrix} = \begin{Bmatrix} \mathbf{0} \\ -\mathbf{E}_\alpha \end{Bmatrix} \tag{9}$$

$$\begin{bmatrix} \mathsf{K}_t & -\mathsf{F} \\ -\mathsf{F}^t & 0 \end{bmatrix} \begin{Bmatrix} \mathbf{u}_{\alpha\beta} \\ \bar{\mathbf{Q}}_{\alpha\beta} \end{Bmatrix} = \begin{Bmatrix} -Q(\mathbf{u}_\alpha,\mathbf{u}_\beta) \\ \mathbf{0} \end{Bmatrix}, \tag{10}$$

where K_t is the tangential stiffness matrix of the full FE model and $\mathbf{E}_\alpha$ is a column vector from the identity matrix of the same size as the number of basis vectors chosen. The side product of solving these systems yields the tensors $\bar{\mathsf{L}}$ and $\bar{\mathsf{Q}}$. The components of $\bar{\mathsf{C}}$ are obtained from:

$$\bar{C}_{\alpha\beta\gamma\delta} = C(\mathbf{u}_\alpha,\mathbf{u}_\beta,\mathbf{u}_\gamma,\mathbf{u}_\delta) - \frac{2}{3}[\mathbf{u}_{\alpha\beta}^t\mathcal{L}(\mathbf{u}_{\delta\gamma}) + \mathbf{u}_{\beta\gamma}^t\mathcal{L}(\mathbf{u}_{\delta\alpha}) + \mathbf{u}_{\gamma\alpha}^t\mathcal{L}(\mathbf{u}_{\delta\beta})]. \tag{11}$$

The subsequent section shows the theoretical formulation of the ROM through adaptation of the Koiter-Newton method.

2.2. The Momentum Subspace Method

In this section a reduced-order model for geometrically nonlinear vibrations is introduced. The inspiration for extending the reduction method from statics to dynamics stems from D'Alembert's principle, as expressed by:

$$F + (-\dot{p}) = kq. \tag{12}$$

Equation 12 states that the addition of the external force F and the inertia term $-\dot{p}$, where $\dot{p}$ is the time derivative of the momentum, are equal to a static term, in which k is the stiffness and q is the displacement. This can be interpreted as that when the motions of the system are known, the static forces are known. Thus if the dynamics are known, they can be reduced to statics. To this extent an assumption is made for the momentum of the system:

$$\mathbf{p} = \mathbf{M}\left[\boldsymbol{\Phi}_1 \;\; \boldsymbol{\Phi}_2 \;\; \boldsymbol{\Phi}_3 \ldots \boldsymbol{\Phi}_n\right]\boldsymbol{\pi}, \tag{13}$$

where, in the present work, $\boldsymbol{\Phi}_n$ are the selected eigenmodes for the formulation of the ROM. However, it is notable that a basis matrix derived from any other method can also be used. $\mathbf{M}$ is the mass matrix, and $\boldsymbol{\pi}$ represents the amplitude, to be determined later. In this work the number of modes (or other basis vectors) used in the basis is referred to as how many degrees of freedom the reduced-order model has, e.g. if one mode is used in the basis it is referred to as a single degree of freedom model. The size of the ROM is determined by the linear transformation in momentum as described by Equation 14. The assumption implies that the momentum of the system is assumed to be defined by a linear subspace. Since, $\mathbf{p}$ is defined by a linear subspace, $\dot{\mathbf{p}}$ is in the same subspace. The assumption for the momentum essentially states that the forces are in this same subspace. The more general case for the momentum subspace is written as:

$$\mathbf{p} = \mathsf{P}\boldsymbol{\pi}, \tag{14}$$

where P is the basis matrix, which is formed from the sub-momentum vectors P_δ. The coordinates π, represent the amplitudes of the sub-momentum vectors.

The overall shape of the motion of the system is thus described by a momentum subspace. The displacement is expanded in a Taylor series of second order as given by Equation 15, which follows the procedure in [23] and [28].

$$\mathbf{q} = \mathbf{q}_0 + \mathbf{u}_\alpha \xi_\alpha + \mathbf{u}_{\alpha\beta}\xi_\alpha\xi_\beta. \tag{15}$$

For plane structures in dynamics the first order displacement field $\mathbf{u}_\alpha$ is associated with the out-of-plane motion, whereas the second order displacement field $\mathbf{u}_{\alpha\beta}$ is associated with the in-plane motion. $\mathbf{q}_0$ is the displacement of the system in the nominal configuration about which one can expand the generic displacement field at any load amplitude. In this work the nominal configuration is assumed to be the undeformed configuration, implying $\mathbf{q}_0$ is zero.
To construct a reduced system, i.e. a system with less degrees of freedom, the number of entries of the amplitude vectors $\boldsymbol{\pi}$ and $\boldsymbol{\xi}$ should be less than the number of degrees of freedom in the original system.
The transformation of coordinates is written as:

$$\mathbf{u} = \mathbf{u}(\boldsymbol{\xi}) = \mathbf{u}_\alpha\xi_\alpha + \mathbf{u}_{\alpha\beta}\xi_\alpha\xi_\beta + \mathbf{u}_{\alpha\beta\gamma}\xi_\alpha\xi_\beta\xi_\gamma \tag{16a}$$

$$\mathbf{p} = \mathbf{p}(\boldsymbol{\pi}) = \mathsf{P}\boldsymbol{\pi} = \mathsf{P}_\delta\boldsymbol{\pi}_\delta. \tag{16b}$$

The amplitude vectors $\boldsymbol{\xi}$ and $\boldsymbol{\pi}$ represent the position and momentum of the reduced-order model and are the equivalent of $\mathbf{u}$ and $\mathbf{p}$ in the original model. Note that the displacement in Equation 16a is expanded in a Taylor series of third order, contrary to Equation 15, which was of second order. The third order expansion merely has a function to later derive the constraint equations and the four-dimensional tensor $\bar{\mathsf{C}}$ for the reduced-order model. The description of the dynamics of the system by the position and momentum makes it convenient to employ the Hamiltonian formulation. However, the transformed system, described by Equation 16, is only a Hamiltonian system if the transformation is canonical. To prove this, Hamilton's principle in the Hamiltonian setting is derived first. Hamilton's equations can be written in a similar form as D'Alembert's principle, although instead of one equation there are now two:

$$p_i - m_i\dot{u}_i = 0 \tag{17a}$$

$$F_i - \dot{p}_i = 0. \tag{17b}$$

These equations are equivalent to Hamilton's equations of motion. The virtual work is computed by multiplying the first canonical equation of Hamilton by δp_i and the second one by δu_i:

$$\dot{u}_i \cdot \delta p_i = \frac{\partial H}{\partial p_i} \cdot \delta p_i \tag{18a}$$

$$\dot{p}_i \cdot \delta u_i = -\frac{\partial H}{\partial q_i} \cdot \delta u_i, \tag{18b}$$

where H represents the Hamiltonian. The second of these equations is subtracted from the first one:

$$\dot{u}_i \cdot \delta p_i - \dot{p}_i \cdot \delta u_i = \frac{\partial H}{\partial p_i} \cdot \delta p_i + \frac{\partial H}{\partial u_i} \cdot \delta u_i. \tag{19}$$

The right hand side of Equation 19 represents the variation of the Hamiltonian δH. Integrating between two time states t_1 and t_2, one obtains Hamilton's principle in the Hamiltonian setting:

$$\int_{t_1}^{t_2} (\delta H + \dot{p}_i \cdot \delta u_i - \dot{u}_i \cdot \delta p_i)\, \mathrm{d}t = 0. \tag{20}$$

A canonical transformation ensures that the form of the term $\dot{\mathbf{p}} \cdot \delta \mathbf{u} - \dot{\mathbf{u}} \cdot \delta \mathbf{p}$ is conserved. A general transformation is performed given by:

$$\mathbf{u} = \mathbf{u}(\boldsymbol{\xi}, \boldsymbol{\pi}) \tag{21a}$$

$$\mathbf{p} = \mathbf{p}(\boldsymbol{\xi}, \boldsymbol{\pi}). \tag{21b}$$

Substituting this transformation in the term whose form is to be conserved, the conditions for a canonical transformation are derived:

$$\begin{aligned}
&\dot{\mathbf{p}}^t \delta \mathbf{u} - \dot{\mathbf{u}}^t \delta \mathbf{p} = \\
&\left[\left(\frac{\partial \mathbf{p}}{\partial \boldsymbol{\xi}}\right)^t \cdot \left(\frac{\partial \mathbf{u}}{\partial \boldsymbol{\xi}}\right) - \left(\frac{\partial \mathbf{u}}{\partial \boldsymbol{\xi}}\right)^t \cdot \left(\frac{\partial \mathbf{p}}{\partial \boldsymbol{\xi}}\right)\right] \cdot \dot{\boldsymbol{\xi}}^t \delta \boldsymbol{\xi} + \\
&\left[\left(\frac{\partial \mathbf{p}}{\partial \boldsymbol{\pi}}\right)^t \cdot \left(\frac{\partial \mathbf{u}}{\partial \boldsymbol{\pi}}\right) - \left(\frac{\partial \mathbf{u}}{\partial \boldsymbol{\pi}}\right)^t \cdot \left(\frac{\partial \mathbf{p}}{\partial \boldsymbol{\pi}}\right)\right] \cdot \dot{\boldsymbol{\pi}}^t \delta \boldsymbol{\pi} + \\
&\left[\left(\frac{\partial \mathbf{u}}{\partial \boldsymbol{\xi}}\right)^t \cdot \left(\frac{\partial \mathbf{p}}{\partial \boldsymbol{\pi}}\right) - \left(\frac{\partial \mathbf{p}}{\partial \boldsymbol{\xi}}\right)^t \cdot \left(\frac{\partial \mathbf{u}}{\partial \boldsymbol{\pi}}\right)\right] \\
&\cdot \left(\dot{\boldsymbol{\pi}}^t \delta \boldsymbol{\xi} - \dot{\boldsymbol{\xi}}^t \delta \boldsymbol{\pi}\right).
\end{aligned} \tag{22}$$

For the transformation to be canonical, the terms between square brackets should be:

$$\left[\left(\frac{\partial \mathbf{p}}{\partial \boldsymbol{\xi}}\right)^t \cdot \left(\frac{\partial \mathbf{u}}{\partial \boldsymbol{\xi}}\right) - \left(\frac{\partial \mathbf{u}}{\partial \boldsymbol{\xi}}\right)^t \cdot \left(\frac{\partial \mathbf{p}}{\partial \boldsymbol{\xi}}\right)\right] = \mathbf{0} \tag{23a}$$

$$\left[\left(\frac{\partial \mathbf{p}}{\partial \boldsymbol{\pi}}\right)^t \cdot \left(\frac{\partial \mathbf{u}}{\partial \boldsymbol{\pi}}\right) - \left(\frac{\partial \mathbf{u}}{\partial \boldsymbol{\pi}}\right)^t \cdot \left(\frac{\partial \mathbf{p}}{\partial \boldsymbol{\pi}}\right)\right] = \mathbf{0} \tag{23b}$$

$$\left[\left(\frac{\partial \mathbf{u}}{\partial \boldsymbol{\xi}}\right)^t \cdot \left(\frac{\partial \mathbf{p}}{\partial \boldsymbol{\pi}}\right) - \left(\frac{\partial \mathbf{p}}{\partial \boldsymbol{\xi}}\right)^t \cdot \left(\frac{\partial \mathbf{u}}{\partial \boldsymbol{\pi}}\right)\right] = \mathbf{I}. \tag{23c}$$

The derivation of the above conditions is found in Appendix A. These conditions can be compared to any literature on classical mechanics such as [31] and [32], in which the same conditions are presented. If these conditions hold, then one obtains:

$$\dot{\mathbf{p}}^t \delta \mathbf{u} - \dot{\mathbf{u}}^t \delta \mathbf{p} = \dot{\boldsymbol{\pi}}^t \delta \boldsymbol{\xi} - \dot{\boldsymbol{\xi}}^t \delta \boldsymbol{\pi}, \tag{24}$$

from which it is seen that the form of the term in the original system is conserved. The resulting transformed system is thus a Hamiltonian system, implying that Hamilton's equations of motion are applicable. Taking into account the

particular transformation performed in this work, as given by Equation 16, the first two conditions of Equation 23 are satisfied, whereas the third condition reduces to:

$$\left(\frac{\partial \mathbf{u}}{\partial \xi_a}\right)^t \cdot \left(\frac{\partial \mathbf{p}}{\partial \pi_b}\right) = \delta_{ab}. \tag{25}$$

The condition of Equation 25 is expanded by substituting the expression for the displacement and momentum, from Equation 16, and performing the differentiation, which yields:

$$\left(\mathbf{u}_a + 2\mathbf{u}_{a\beta}\xi_\beta + 3\mathbf{u}_{a\beta\gamma}\xi_\beta\xi_\gamma\right)^t \cdot \mathsf{P}_b = \delta_{ab}. \tag{26}$$

This equation is satisfied if the following three constraint equations hold:

$$\begin{cases} \mathsf{P}_\delta^t \mathbf{u}_\alpha = \delta_{\alpha\delta} & \text{(27a)} \\ \mathsf{P}_\delta^t \mathbf{u}_{\alpha\beta} = 0 & \text{(27b)} \\ \mathsf{P}_\delta^t \mathbf{u}_{\alpha\beta\gamma} = 0. & \text{(27c)} \end{cases}$$

At this point the analogy to the reduction method for statics, as discussed in [28], is made. The constraints given by Equation 27 are of the same form as the constraint equations for the reduction method for statics, given by Equation 7. The only difference between the two is that the sub-load vectors $\mathbf{f}_\alpha$ are replaced with the sub-momentum vectors P_δ. This convenient analogy reduces the dynamic case to the static case, which implies that the reduced-order model as developed by Liang [28] is directly applicable to dynamics.
To formulate the equations of motion of the system, use is made of the Hamiltonian. For natural Hamiltonian systems the Hamiltonian is computed by the addition of the kinetic energy T and the potential energy V:

$$H(\mathbf{u}, \mathbf{p}) = T(\mathbf{u}, \mathbf{p}) + V(\mathbf{u}). \tag{28}$$

In this work a constant mass matrix is assumed and the kinetic energy merely depends on the momentum. The Hamiltonian is calculated by:

$$H(\mathbf{u}, \mathbf{p}) = \frac{1}{2}\mathbf{p}^t\mathbf{M}^{-1}\mathbf{p} + V(\mathbf{u}). \tag{29}$$

For the reduced-order model, the Hamiltonian (or reduced Hamiltonian) is a function of $\boldsymbol{\xi}$ and $\boldsymbol{\pi}$. For the computation of the kinetic energy, use is made of the momentum subspace given by Equation 13. The potential energy is computed by integrating Equation 8 for the load amplitudes. The kinetic and potential energy are given by:

$$\bar{T} = \frac{1}{2}\boldsymbol{\pi}^t\left(\mathsf{P}^t\mathbf{M}^{-1}\mathsf{P}\right)\boldsymbol{\pi} \tag{30a}$$

$$\bar{V} = \frac{1}{2}\bar{L}_{\alpha\beta}\xi_\alpha\xi_\beta + \frac{1}{3}\bar{Q}_{\alpha\beta\gamma}\xi_\alpha\xi_\beta\xi_\gamma + \frac{1}{4}\bar{C}_{\alpha\beta\gamma\delta}\xi_\alpha\xi_\beta\xi_\gamma\xi_\delta. \tag{30b}$$

If the basis matrix is taken to be $\mathbf{M}\cdot\boldsymbol{\Phi}$, with $\boldsymbol{\Phi}$ being the modal matrix, one can simplify the reduced Hamiltonian and compute a reduced mass matrix. Substituting this expression for P, the kinetic energy simplifies to:

$$\bar{T} = \frac{1}{2}\boldsymbol{\pi}^t\left(\boldsymbol{\Phi}^t\mathbf{M}\boldsymbol{\Phi}\right)\boldsymbol{\pi}. \tag{31}$$

The reduced mass matrix is identified to be $\bar{\mathbf{M}} = \left(\boldsymbol{\Phi}^t\mathbf{M}\boldsymbol{\Phi}\right)^{-1}$.
Finally, the Hamiltonian of the reduced-order model becomes:

$$\bar{H} = \bar{T} + \bar{V}. \tag{32}$$

This reduced Hamiltonian still represents a mechanical system, since the transformation of the original position and momentum coordinates $\mathbf{u}$ and $\mathbf{p}$ to the new set of coordinates $\boldsymbol{\xi}$ and $\boldsymbol{\pi}$, is canonical.

Hamilton's canonical equations of motion are applied to obtain $2\bar{n}$ coupled differential equations, of first order for the position and momentum coordinates. It is assumed that a modal basis is used and the basis matrix is $\mathsf{P} = \mathbf{M}\mathbf{\Phi}$. The $2\bar{n}$ first order ordinary differential equations can be written as:

$$\dot{\boldsymbol{\xi}} = \frac{\partial \bar{H}}{\partial \boldsymbol{\pi}} = \bar{\mathbf{M}}^{-1}\boldsymbol{\pi} \tag{33a}$$

$$\dot{\boldsymbol{\pi}} = -\frac{\partial \bar{H}}{\partial \boldsymbol{\xi}} = -\left\{\bar{\mathcal{L}}(\boldsymbol{\xi}) + \bar{\mathcal{Q}}(\boldsymbol{\xi},\boldsymbol{\xi}) + \bar{C}(\boldsymbol{\xi},\boldsymbol{\xi},\boldsymbol{\xi})\right\}, \tag{33b}$$

which holds for free vibrations. To account for time-varying loads a forcing term is added. The reduced force is computed through:

$$\bar{\boldsymbol{\phi}}(t) = \mathbf{u}_{\alpha}^{t}\mathbf{f}_{ex}. \tag{34}$$

To simulate damping, we make use of Rayleigh damping. For the reduced-order model a reduced damping matrix $\bar{\mathbf{C}}$ is defined as:

$$\bar{\mathbf{C}} = \bar{\mathbf{M}}\left(\mathsf{P}^{t}\mathbf{M}^{-1}\mathbf{C}\mathbf{M}^{-1}\mathsf{P}\right)\bar{\mathbf{M}}. \tag{35}$$

The canonical equations of motion are slightly modified to incorporate Rayleigh damping. Damping is non-conservative and thus the Hamiltonian is not conserved. A Hamiltonian with damping is therefore called a perturbed Hamiltonian as pointed out in [33]. The canonical equations of motion for forced vibrations of a damped system are given by:

$$\dot{\boldsymbol{\xi}} = \frac{\partial \bar{H}}{\partial \boldsymbol{\pi}} = \bar{\mathbf{M}}^{-1}\boldsymbol{\pi} \tag{36a}$$

$$\dot{\boldsymbol{\pi}} = -\frac{\partial \bar{H}}{\partial \boldsymbol{\xi}} = -\left\{\bar{\mathcal{L}}(\boldsymbol{\xi}) + \bar{\mathcal{Q}}(\boldsymbol{\xi},\boldsymbol{\xi}) + \bar{C}(\boldsymbol{\xi},\boldsymbol{\xi},\boldsymbol{\xi})\right\} - \bar{\mathbf{C}}\bar{\mathbf{M}}^{-1}\boldsymbol{\pi} + \bar{\boldsymbol{\phi}}(t). \tag{36b}$$

After integrating the equations of motion, the response of the original model, in terms of $\mathbf{u}$ and $\mathbf{p}$, is obtained by applying Equation 14 and Equation 15. These equations link the response of the reduced-order model to the response of the full finite element model. A similar form of the equation of motion with cubic nonlinearity in stiffness has also been used in [34], albeit in the Euler-Lagrange form.

The ROM formulation requires computations of tangent stiffness matrix for initial configuration of the structure, and higher order stiffness tensors for the high fidelity FE model. These properties are inherent to the structural FE model when coupled with an FE tool capable of computing the higher order stiffness tensors. Furthermore, additional computations for the basis are required. In the case of a modal basis, this can be obtained by a simple eigenvalue analysis since only a linear transformation is used in the momentum space. The primary cost is incurred in computing the ROM stiffness tensors $\bar{\mathsf{L}}$, $\bar{\mathsf{Q}}$ and $\bar{\mathsf{C}}$. This is, to some extent, affected by the fidelity of the full-scale FE model and the complexity of the model since this determines the size of the coefficient matrices in Equation 9 and Equation 10.For example, by increasing the fidelity of the initial full-scale FE model from 2040 elements to 5040 elements, the ROM formulation time increases by a factor of 2.4. Although, the formulation times are still in fractions of a minute, it can be expected to increase further with the complexity of the model. The ROM formulation is based on the initial configuration of the structure and is therefore, computed only once in the formulation procedure.

2.3. Finite Element Implementation

For the finite element implementation we use the triangular three-node flat shell element. It is a combination of a membrane element and a bending element, as shown in Figure 2. The membrane part contains the in-plane degrees of freedom, and the bending part the out-of-plane degrees of freedom. In total it has six degrees of freedom per node as given by:

$$\mathbf{q}_i = \begin{bmatrix} u_i & v_i & w_i & \theta_{x_i} & \theta_{y_i} & \theta_{z_i} \end{bmatrix}. \tag{37}$$

where $i = 1, 2, 3$, denotes the node numbers. The total degrees of freedom are assembled in a vector:

$$\mathbf{q} = \begin{bmatrix} \mathbf{q}_1 & \mathbf{q}_2 & \mathbf{q}_3 \end{bmatrix}^{t}. \tag{38}$$

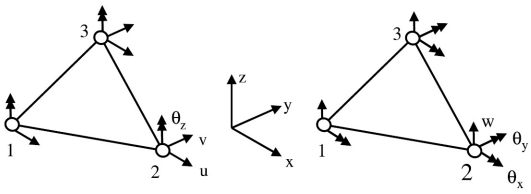

Figure 2: Three-node flat shell element, membrane (left) and bending (right) degrees of freedom [23]

,

2.3.1. Strain definitions

The curvatures are linear with respect to the displacement. For this reason the in-plane strain ϵ will only be considered. The in-plane strain is split into two parts, which is a linear and a nonlinear part. More specifically, it is expressed as:

$$\epsilon = \epsilon_l + \epsilon_{nl} = \left(\mathsf{B}_l + \frac{1}{2}\mathsf{B}_{nl}(\mathbf{q})\right)\mathbf{q} = \mathsf{B}_l\mathbf{q} + \frac{1}{2}\mathbf{q}^t\mathsf{S}\mathbf{q}. \tag{39}$$

In this paper the following expression for the total B matrix is adopted:

$$\mathsf{B}(\mathbf{q}) = \mathsf{B}_l + \mathsf{B}_{nl}(\mathbf{q}). \tag{40}$$

The expression for B_l is found in Appendix B.

2.3.2. Linear stiffness matrix

The linear strain-displacement matrix B_l allows one to directly compute the membrane part of the stiffness matrix through:

$$\begin{aligned} K_{in-plane} &= K_{b_{in-plane}} + K_{h_{in-plane}} \\ &= A\mathsf{B}_l^t\mathsf{A}_m\mathsf{B}_l + K_{h_{in-plane}}. \end{aligned} \tag{41}$$

The stiffness matrix is composed of a so-called basic stiffness matrix, and a higher order stiffness matrix. The basic stiffness matrix ensures convergence, whereas the higher order stiffness matrix is for stability. Explicit expressions for the computation of the latter one is found in [35]. The same holds for the bending part of the stiffness matrix of which the derivation is found in [36].

2.3.3. Material matrix

A_m and D_b are the material matrices of an isotropic material for membrane and bending, respectively.

$$\mathsf{A}_m = \frac{Eh}{1-\nu^2}\begin{bmatrix} 1 & \nu & 0 \\ \nu & 1 & 0 \\ 0 & 0 & \frac{1-\nu}{2} \end{bmatrix} \tag{42a}$$

$$\mathsf{D}_b = \frac{Eh^3}{12(1-\nu^2)}\begin{bmatrix} 1 & \nu & 0 \\ \nu & 1 & 0 \\ 0 & 0 & \frac{1-\nu}{2} \end{bmatrix} \tag{42b}$$

2.3.4. Nonlinear in-plane strain and stress resultants

Expressions for ϵ_{nl}, $\mathsf{B}_{nl}(\mathbf{q})$ and S are given by Equation 43 to Equation 45 and are computed by using the matrices K_{xx}, K_{yy} and K_{xy}. These constant matrices are obtained from [23] and expressions for them can be found in Appendix B.

$$\epsilon_{nl}(\mathbf{q},\mathbf{q}) = \frac{1}{2}\begin{bmatrix} \mathbf{q}^t\mathsf{K}_{xx}\mathbf{q} \\ \mathbf{q}^t\mathsf{K}_{yy}\mathbf{q} \\ \mathbf{q}^t\mathsf{K}_{xy}\mathbf{q} \end{bmatrix} \tag{43}$$

$$\mathsf{B}_{nl}(\mathbf{q}) = \frac{\partial \epsilon_{nl}}{\partial \mathbf{q}} = \begin{bmatrix} \mathbf{q}^t \mathsf{K}_{xx} \\ \mathbf{q}^t \mathsf{K}_{yy} \\ \mathbf{q}^t \mathsf{K}_{xy} \end{bmatrix} \tag{44}$$

$$\mathsf{S} = \frac{\partial^2 \epsilon_{nl}}{\partial \mathbf{q}^2} = \begin{bmatrix} \mathsf{S}(1,:,:) = \mathsf{K}_{xx} \\ \mathsf{S}(2,:,:) = \mathsf{K}_{yy} \\ \mathsf{S}(3,:,:) = \mathsf{K}_{xy} \end{bmatrix} \tag{45}$$

S is a 3×3×3 tensor, with $\mathsf{S}(a,:,:)$ indicating the a-th two-dimensional matrix in S. The in-plane stress resultant is obtained by multiplying the strain by the material matrix. This is split into a linear and nonlinear part:

$$\begin{aligned} \mathbf{N} &= \mathsf{A}_m \left(\mathsf{B}_l + \frac{1}{2} \mathsf{B}_{nl}(\mathbf{q}) \right) \mathbf{q} \\ &= \mathsf{A}_m \mathsf{B}_l \mathbf{q} + \frac{1}{2} \mathsf{A}_m \mathsf{B}_{nl}(\mathbf{q}) \mathbf{q} \\ &= \mathbf{N}_l + \mathbf{N}_{nl}. \end{aligned} \tag{46}$$

2.3.5. In-plane strain energy and the reduced-order model

Using the index notation, the in-plane strain energy is computed as:

$$U_{in-plane} = \frac{1}{2} \mathcal{A} \mathsf{A}_{m_{\alpha\beta}} (\epsilon_{l_\alpha} + \epsilon_{nl_\alpha})(\epsilon_{l_\beta} + \epsilon_{nl_\beta}). \tag{47}$$

The subscripts $\alpha, \beta = 1, 2, 3$ refer to the components in the tensor and $\mathcal{A}$ is the area of the shell element. The nonlinear part of the strain energy is defined by:

$$U = \frac{1}{2} \mathcal{A} \mathsf{A}_{m_{\alpha\beta}} (2\epsilon_{l_\alpha} \epsilon_{nl_\beta} + \epsilon_{nl_\alpha} \epsilon_{nl_\beta}) \tag{48}$$

The internal force vector f_i and the tangential stiffness matrix L_{ij} are found by differentiating the in-plane strain energy up to first and second order, respectively:

$$\begin{aligned} f_i &= \frac{\partial U}{\partial q_i} \\ &= \frac{\mathcal{A} \mathsf{A}_{m_{\alpha\beta}}}{2} \Big(2 \frac{\partial \epsilon_{l_\alpha}}{\partial q_i} \epsilon_{nl_\beta} + \frac{\partial \epsilon_{nl_\beta}}{\partial q_i} \epsilon_{nl_\alpha} + \frac{\partial \epsilon_{nl_\alpha}}{\partial q_i} \epsilon_{nl_\beta} \\ &\qquad + 2 \frac{\partial \epsilon_{nl_\beta}}{\partial q_i} \epsilon_{l_\alpha} \Big) \end{aligned} \tag{49}$$

$$\begin{aligned} L_{ij} &= \frac{\partial^2 U}{\partial q_i \partial q_j} \\ &= \mathcal{A} \mathsf{A}_{m_{\alpha\beta}} \Big(\frac{\partial \epsilon_{l_\alpha}}{\partial q_i} \frac{\partial \epsilon_{nl_\beta}}{\partial q_j} + \frac{\partial \epsilon_{l_\alpha}}{\partial q_j} \frac{\partial \epsilon_{nl_\beta}}{\partial q_i} + \\ &\qquad \frac{\partial^2 \epsilon_{nl_\alpha}}{\partial q_i \partial q_j} \epsilon_{nl_\beta} + \frac{\partial^2 \epsilon_{nl_\beta}}{\partial q_i \partial q_j} \epsilon_{l_\alpha} + \frac{\partial \epsilon_{nl_\alpha}}{\partial q_i} \frac{\partial \epsilon_{nl_\beta}}{\partial q_j} \Big), \end{aligned} \tag{50}$$

where the indices are $i, j = 1, \ldots, 18$ and the Einstein summation convention is applied over the indices α and β. With the aid of the expression from the previous sections, a more compact form is obtained:

$$\mathbf{f} = \mathcal{A} \left(\mathsf{B}_l^t \mathbf{N}_{nl} + \mathsf{B}_{nl}^t \mathbf{N} \right) \tag{51}$$

$$\mathsf{L} = \mathcal{A} (\mathsf{B}_l^t \mathsf{A}_m \mathsf{B}_{nl} + \mathsf{B}_{nl}^t \mathsf{A}_m \mathsf{B}_l + \mathsf{B}_{nl}^t \mathcal{A}_m \mathsf{B}_{nl} + N_x \mathsf{K}_{xx} + N_y \mathsf{K}_{yy} + N_{xy} \mathsf{K}_{xy}), \tag{52}$$

where L is equal to the tangential stiffness matrix K_t. N_x, N_y and N_{xy} refer to the three components of the stress resultant vector $\mathbf{N}$. Q and C are obtained by differentiating the in-plane strain energy up to third and fourth order, respectively.

However, a simpler way is to directly obtain $Q(\mathbf{u}_\alpha, \mathbf{u}_\beta)$, used in Equation 10, by multiplying Equation 51 with $\mathbf{u}_\alpha^t$ and $\mathbf{u}_\beta$ and then to differentiate with respect to the degrees of freedom. To this extent two compact notations are introduced. The stress resultant related to the displacement $\mathbf{u}_\alpha$, and the stress resultant depending on the first order displacement fields $\mathbf{u}_\alpha$ and $\mathbf{u}_\beta$ are defined by:

$$\begin{cases} \overline{\mathbf{N}}(\mathbf{u}_\alpha) = \mathsf{A}_m \mathsf{B}(\mathbf{u}_\alpha)\mathbf{u}_\alpha \\ \overline{\overline{\mathbf{N}}}(\mathbf{u}_\alpha, \mathbf{u}_\beta) = \mathsf{A}_m \mathsf{B}_{nl}(\mathbf{u}_\alpha)\mathbf{u}_\beta. \end{cases} \tag{53}$$

The expression of $Q(\mathbf{u}_\alpha, \mathbf{u}_\beta)$ for the shell element would then be:

$$Q(\mathbf{u}_\alpha, \mathbf{u}_\beta) = \frac{\mathcal{A}}{2}(\mathsf{B}_{nl}^t(\mathbf{u}_\beta)\overline{\mathbf{N}}(\mathbf{u}_\alpha) + \mathsf{B}_{nl}^t(\mathbf{u}_\alpha)\overline{\mathbf{N}}(\mathbf{u}_\beta) + \mathsf{B}^t\overline{\overline{\mathbf{N}}}(\mathbf{u}_\alpha, \mathbf{u}_\beta)). \tag{54}$$

The term $C(\mathbf{u}_\alpha, \mathbf{u}_\beta, \mathbf{u}_\gamma, \mathbf{u}_\delta)$ in Equation 11 is computed by multiplying Equation 54 by the first order displacement field $\mathbf{u}_\gamma^t$, then differentiating it with respect to the degrees of freedom, and then multiplying it by $\mathbf{u}_\delta$. Furthermore, the following compact notation is used:

$$\mathbf{m}(\mathbf{u}_\alpha, \mathbf{u}_\beta) = \mathsf{B}_{nl}(\mathbf{u}_\alpha)\mathbf{u}_\beta \tag{55}$$

$$C(\mathbf{u}_\alpha, \mathbf{u}_\beta, \mathbf{u}_\gamma, \mathbf{u}_\delta) = \frac{\mathcal{A}}{6}[\overline{\overline{\mathbf{N}}}(\mathbf{u}_\alpha, \mathbf{u}_\delta)\mathbf{m}(\mathbf{u}_\beta, \mathbf{u}_\gamma) + \overline{\overline{\mathbf{N}}}(\mathbf{u}_\beta, \mathbf{u}_\delta)\mathbf{m}(\mathbf{u}_\alpha, \mathbf{u}_\gamma) + \overline{\overline{\mathbf{N}}}(\mathbf{u}_\gamma, \mathbf{u}_\delta)\mathbf{m}(\mathbf{u}_\alpha, \mathbf{u}_\beta)]. \tag{56}$$

Expressions for L (Equation 52) and $Q(\mathbf{u}_\alpha, \mathbf{u}_\beta)$ (Equation 54) have been obtained. They are used in the linear systems of equations, Equation 9 and Equation 10, to obtain the first and second order displacement fields as well as $\bar{\mathcal{L}}$ and $\bar{Q}$ in the reduced-order model. $C(\mathbf{u}_\alpha, \mathbf{u}_\beta, \mathbf{u}_\gamma, \mathbf{u}_\delta)$ is used to obtain the $\bar{C}$.

3. Solution Methodology

The reduced-order model derived in the subsection 2.2 has been solved using the pseudo-arclength continuation algorithm in AUTO [37]. The originally derived system of equations was modified to make it more suitable for the continuation scheme. The system was transformed to modal coordinates using mass - orthonormalized eigenvectors obtained from linear eigenvalue analysis. This converts the mass matrix to an identity matrix and eliminates one parameter from the computations. Scale factors were introduced to make the system variables displacement, time and force, non-dimensional.

$$\boldsymbol{\xi}^* = \boldsymbol{\xi}/\alpha, \qquad t^* = t/\beta, \qquad \bar{\boldsymbol{\phi}}^* = \bar{\boldsymbol{\phi}}/\gamma, \tag{57}$$

where α, β and γ are the scale factors for displacement, time and force variables, respectively. The non-dimensional variables are substituted back into the governing equations and the scale factors are computed by equating coefficients of terms in the Lagrangian form of the equation of motion.

$$\ddot{\boldsymbol{\xi}}^* + \beta\bar{\mathbf{C}}\dot{\boldsymbol{\xi}}^* + \beta^2\bar{\mathcal{L}}(\boldsymbol{\xi}^*) + \alpha\beta^2\bar{Q}(\boldsymbol{\xi}^*, \boldsymbol{\xi}^*) + \alpha^2\beta^2\bar{C}(\boldsymbol{\xi}^*, \boldsymbol{\xi}^*, \boldsymbol{\xi}^*) = (\beta^2\gamma/\alpha)\bar{\boldsymbol{\phi}}^* \sin(\omega t^*\beta). \tag{58}$$

The scale factors for computing the i$^{\text{th}}$ nonlinear mode are derived from the corresponding diagonal elements of stiffness tensors.

$$\begin{aligned} \alpha_i &= \text{Max}(\sqrt{L_{ii}/C_{iiii}}, L_{ii}/Q_{iii}), \\ \beta_i &= \sqrt{1/L_{ii}} = 1/\omega_{ni}, \\ \gamma_i &= L_{ii}\alpha_i. \end{aligned}$$

The scale factors are used to compute equivalent stiffness tensors and damping matrix using the terms $\beta^2\bar{\mathcal{L}}$, $\alpha\beta^2\bar{Q}$, $\alpha^2\beta^2\bar{C}$ and $\beta\bar{\mathbf{C}}$ from the Equation 58. The governing equations are then formulated in terms of the non- dimensionalized variables and equivalent tensors. The equation set is then solved using the pseudo- arclength continuation which produces displacement response in the normalized and scaled system of equations. To obtain the actual nonlinear response of the structure, the scale factors are re-applied. The peak amplitudes are extracted for each frequency step of the analysis which is used to predict the nonlinear modal frequency.

4. Experiments

An aluminium stiffened plate was manufactured for the experimental study. The plate and the stiffener were manufactured integrally from an aluminium block using CNC milling process to avoid the use of bonding or fastening methods. The dimensions of the plate are: length l = 0.5 m, width w = 0.4 m, thickness t = 0.002 m. The dimensions of the stiffener are: length l_s = 0.4 m, height h_s = 0.008 m, thickness t_s = 0.005 m. The material properties are: Modulus of elasticity E = 70e9 Pa, density = 2660 kg /m^3, Poisson's ratio ν = 0.33. The linear vibration measurements were conducted using a Polytec Scanning Vibrometer (PSV) setup. The objective of these measurements was to get an initial prediction of the modal damping ratios to be used in the numerical analysis. The measurement of linear modal frequency was further used to validate the FE model developed for the numerical analysis. Free boundary conditions were chosen for the analysis of the stiffened plate. To simulate the free boundary condition in the experiments, the stiffened plate was suspended at two points using bungee cords from a supporting frame. The flexibility of the cords ensure a close approximation of the free boundary condition. The test setup is depicted in the Figure 3a.

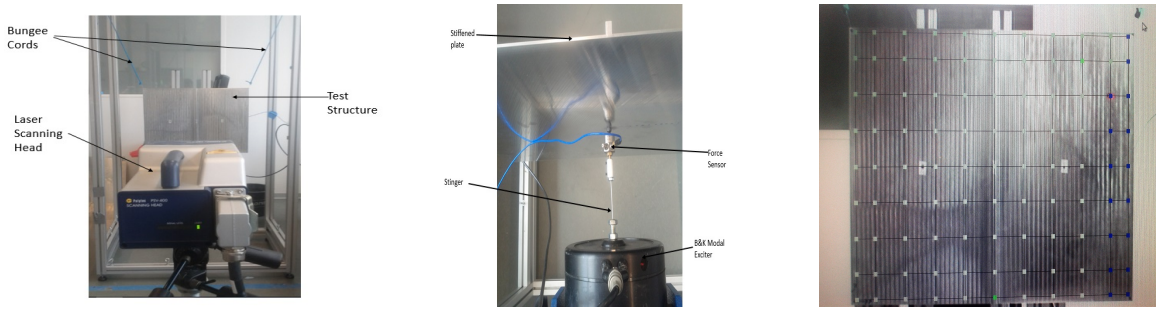

(a) Experimental setup for vibration measurements (b) Stinger assembly (c) Grid defining the measurement points

Figure 3: Components of the experimental setup

The plate was excited using the B&K4809 modal exciter which was connected to the structure using a flexible stinger assembly shown in Figure 3b. To obtain a good prediction of the linear vibration mode shape, ninety-nine measurement points were chosen across the plate using the PSV software, shown in Figure 3c. The measurements for frequencies up to 200 Hz were obtained by applying a random vibration signal to the structure.

The nonlinear vibration measurements were conducted using a combination of the PSV and Mueller BBM PAK MK-II setup. In this setup, the transient vibration data is measured using the PSV laser and the measured data is transferred to the PAK MK-II system for obtaining the frequency vs peak amplitude responses. The measurement was conducted only at the point of maximum deflection which is the corner point of the plate for the first mode. To obtain the frequency vs peak amplitude response curves, a harmonic sweep is applied at a constant load amplitude. The maximum measured amplitude for each frequency step in the sweep provides a single point along the frequency-amplitude response.

5. Results

5.1. Comparison with numerical results

This first example is focused on the performance of the ROM in the time domain in comparison to the commercial finite element package Abaqus. For this a rectangular plate is used with geometrical dimensions: length = 0.3 m, width = 0.2 m and thickness = 0.005 m. The material properties are: a modulus of elasticity of E = 71.7e9 Pa, density ρ = 2810 kg/m^3 and Poisson's ratio ν = 0.33. All edges of the plate are simply supported. A uniform pressure load of the form p=λ sinωt is applied, where λ = 50 N/m^2 and $\omega = 0.9\omega_1$. A damping ratio of 0.036 for the first mode is used. The frequencies of the modes to be used in the basis of the ROM are compared in Table 1. The response at the center of the plate is of interest, therefore modes with an even number of half-waves are excluded and only the first five modes with an odd number of half-waves are considered for building the ROM. The comparison between the ROM and Abaqus for the displacement over time at the center of the plate is shown in Figure 4. It is observed that when two modes are used

Mode number	ROM (Hz)	Abaqus (Hz)
1	43.79	43.82
4	151.79	152.00
8	287.33	288.30
11	368.61	370.14
12	395.24	396.27

Table 1: Comparison of frequencies of the FE framework of the ROM and Abaqus

in the basis of the ROM excellent agreement is found between Abaqus and the ROM. Figure 6a and Figure 6b show the moments over time at the center of the plate in comparison to that of Abaqus. Similar as for the stress resultants, five modes are used in the basis of the ROM to obtain agreement.

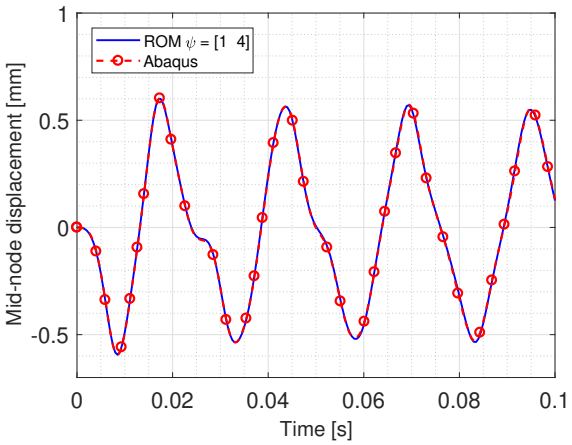

Figure 4: Nonlinear displacement response at the center of the rectangular plate

For further comparison, the complexity of the structural model was increased by using the stiffened plate model, previously described. To test the FE model of the stiffened plate, a nonlinear vibration analysis with sinusoidal loading of 5 N at the center of the plate has been conducted. A modal damping ratio of 0.0407 is used in the analysis while the excitation frequency is 77.98 Hz. The comparison of results from the ROM and Abaqus are found to be in good agreement as shown in Figure 7. Noteworthy is that the ROM has been found to be at least thirty times faster than Abaqus. Initial validation of the nonlinear frequency response curves was obtained by comparison with the literature. The analysis was performed on a rectangular plate with geometrical dimensions: length = 0.3 m , width = 0.3 m, thickness = 0.001 m. The material properties are: Modulus of elasticity E = 70e9 Pa, density ρ = 2778 kg / m^3 and Poisson's ratio ν = 0.3. A harmonic force of F = 1.74 N was applied with a modal damping ratio ζ = 0.065 for the first mode. Using the results of the numerical analysis, a plot of normalized frequency vs peak amplitude was generated for comparison. The results were found to be in excellent agreement with the reference results from [12] and [38]. The comparison is depicted in Figure 8. A convergence study showed that accurate results were obtainable using a one degree of freedom ROM. The second validation was obtained by comparing the numerical nonlinear frequency response of the stiffened plate with the experimental results obtained from the method described in Section 4. The FE model developed using triangular shell elements, as described in Section 2, is depicted in the Figure 9.

5.2. Comparison with experimental results

The modal frequency predictions from linear vibration measurement were compared with the FE modal analysis using the developed numerical model. The error margins were found to be within an acceptable range. The comparison

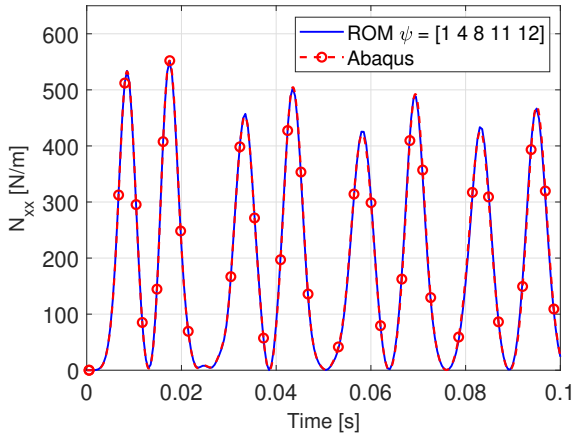

(a) Nonlinear resultant, N_{xx} at the center of the rectangular plate

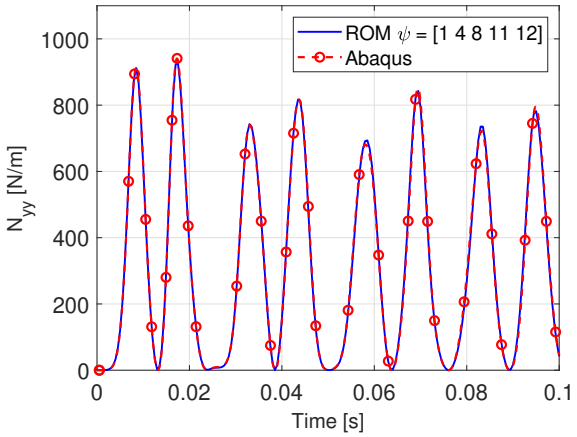

(b) Nonlinear resultant, N_{yy} at the center of the rectangular plate

Figure 5: Nonlinear resultant forces at the center of the rectangular plate

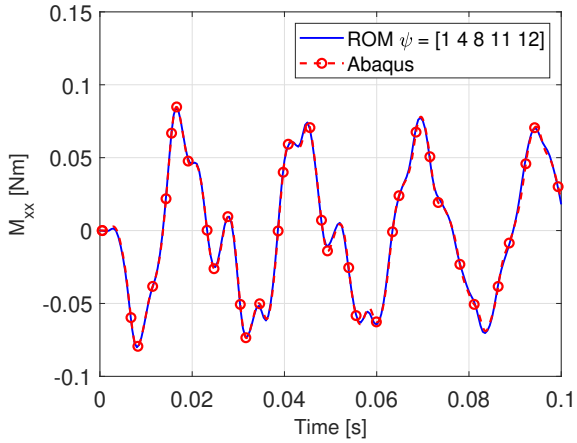

(a) Nonlinear moment, M_{xx} at the center of the rectangular plate

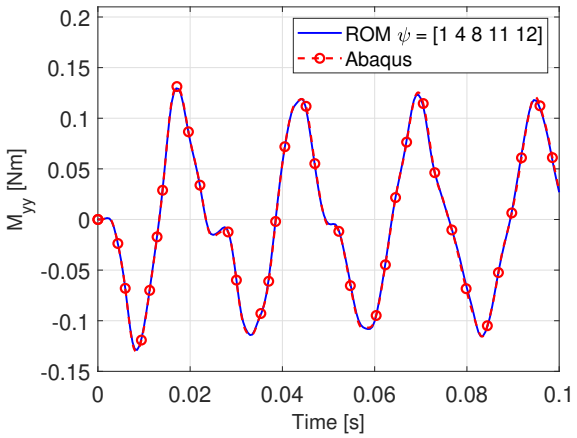

(b) Nonlinear moment, M_{yy} at the center of the rectangular plate

Figure 6: Nonlinear resultant moments at the center of the rectangular plate

along with the computed modal damping ratios is shown in Table 2. The next set of comparisons were made with the results of the nonlinear vibration measurements. Five load cases were chosen for the measurements: 0.2 N, 0.5 N, 0.8 N, 1.0 N, 1.2 N. The harmonic frequency was swept between 32 Hz and 40 Hz i.e. in the near vicinity of the first natural frequency. A distinctive hardening nonlinearity is observable in the frequency vs amplitude response curves obtained experimentally, normalized by the first natural frequency and thickness of the plate, respectively. The nonlinear response for all load cases is depicted in Figure 10. The damping ratio obtained experimentally for the first mode was used as an initial assumption in numerical computations of the nonlinear frequency response curves. The comparisons of the numerical analysis with the experimental results are depicted in Figure 11 - Figure 15.

The numerical results are found to be in good agreement with the experimental results with the use of only a single degree of freedom in the ROM. The analyses were repeated by considering higher number of modes in the ROM, however, the changes seen in the response were negligibly small, as depicted in Figure 16 and Figure 17. The frequency ratios computed by increasing the ROM size in steps of one degree of freedom up to five are: 1.0695, 1.0694, 1.0694, 1.0687, 1.0686. Therefore, a change of only 0.08% is seen by increasing the ROM size to five degree of freedom model. It is notable that the FE model was created with the assumption that the plate is perfectly flat and free of defects.

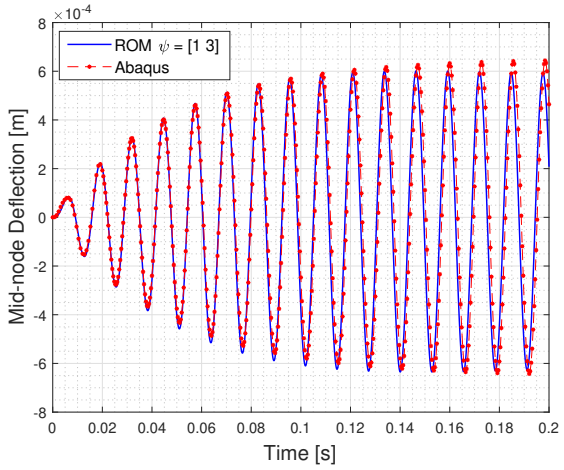

Figure 7: Comparison of ROM with Abaqus for mid-node deflection of stiffened plate in nonlinear vibration

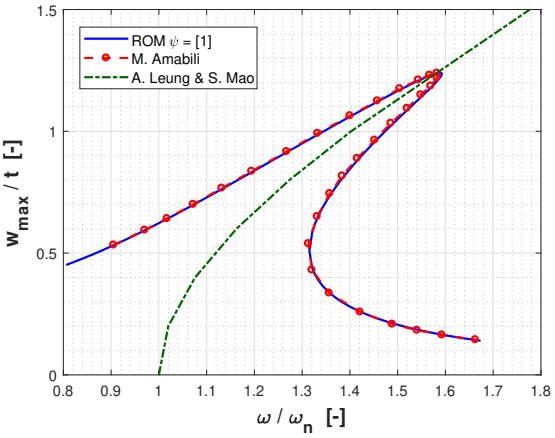

Figure 8: Comparison of nonlinear vibration response for a simple rectangular plate with results of Amabili[38], and Leung & Mao[12]

Mode number	**Exp. modes (Hz)**	**FEM modes (Hz)**	**Error (%)**	**Damp. ratio**
1	35.39	36.78	3.9	0.0012
2	42.97	42.72	-0.58	0.0011
3	77.8	77.59	-0.27	0.00062
4	97.57	94.84	-2.79	0.00068
5	-	97.97	-	-
6	124.7	123.62	-0.86	0.00087
7	161.7	162.4	0.43	0.00067

Table 2: Comparison of modal frequencies:Experimental and numerical

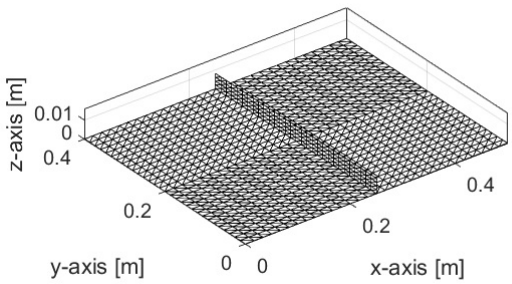

Figure 9: FE model of the stiffened plate

However, presence of any manufacturing imperfection can cause an effect on the nonlinear response of a structure [39]. Therefore, minor variations in results can be possibly attributed to non-observable imperfections in the test structure. Another observation from the numerical computations was the requirement of a variable damping ratio with respect

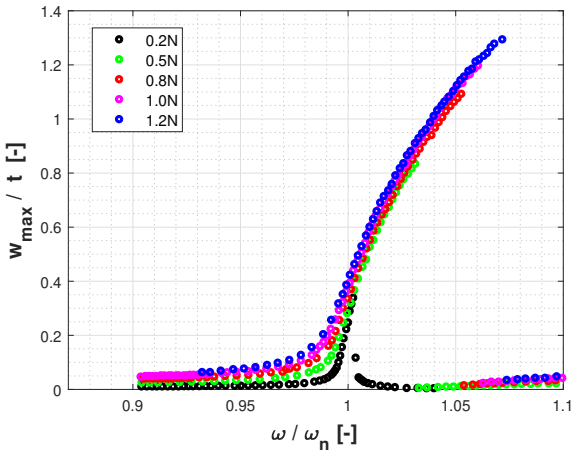

Figure 10: Nonlinear experimental frequency response of stiffened plate for five load amplitudes ranging from 0.2 N to 1.2 N

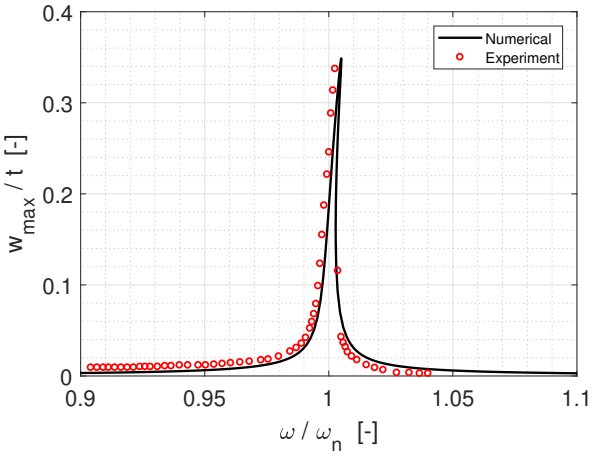

Figure 11: Comparison between experimental and numerical nonlinear frequency response curves of the stiffened plate when f=0.2N and is applied at x=0.2m, y=0.16m

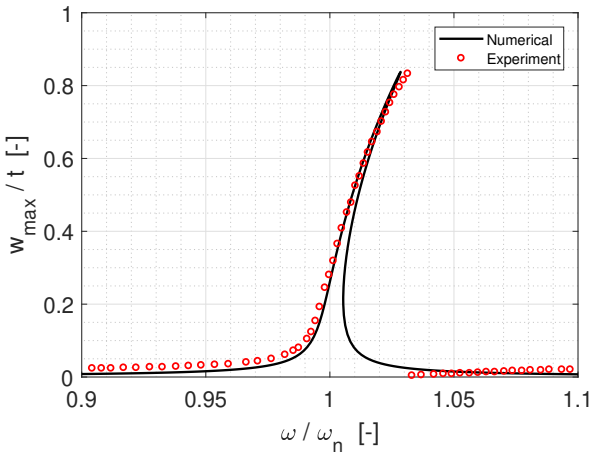

Figure 12: Comparison between experimental and numerical nonlinear frequency response curves of the stiffened plate when f=0.5N and is applied at x=0.2m, y=0.16m

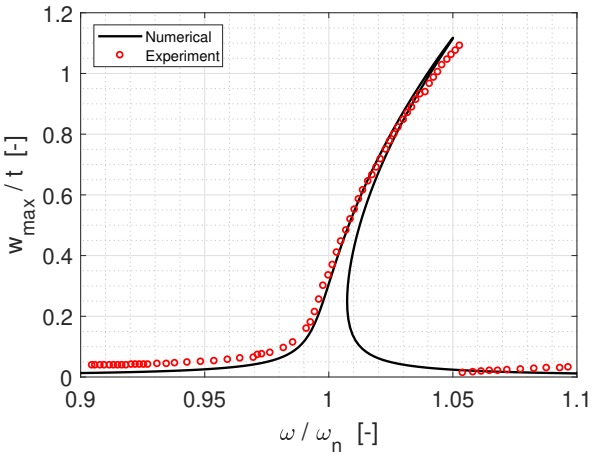

Figure 13: Comparison between experimental and numerical nonlinear frequency response curves of the stiffened plate when f=0.8N and is applied at x=0.2m, y=0.16m

to increasing vibration amplitude, which indicates a requirement of nonlinear damping model [40, 41]. The modal damping ratio of the first mode predicted from linear vibration experiments was insufficient to correctly predict the nonlinear numerical response at higher vibration amplitudes. This behaviour, however, is in agreement with the results obtained in [42] and [43]. The variation of damping ratio with the applied load amplitude in measurements is depicted in Figure 18.

6. Conclusions

A numerical formulation for model reduction in structural dynamics has been proposed in the Hamiltonian framework with the possibility of utilizing any generic ROM basis. It has been shown that the transformation to a reduced system in the Hamiltonian form is canonical, therefore, conserving the properties of the system. An FE formulation has been used to develop a test model compatible with the model reduction algorithm. The ROM is an extension of the reduction

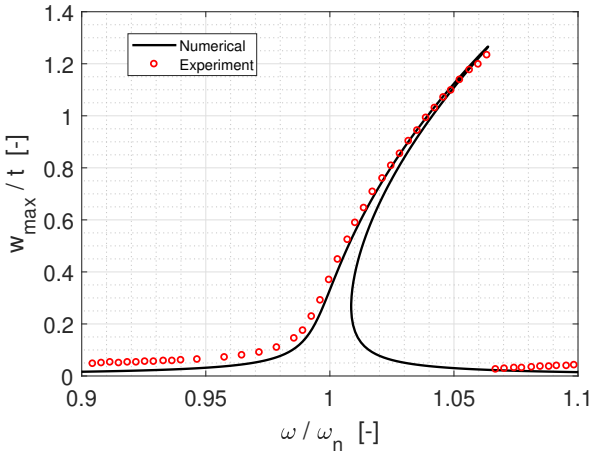

Figure 14: Comparison between experimental and numerical nonlinear frequency response curves of the stiffened plate when f=1.0N and is applied at x=0.2m, y=0.16m

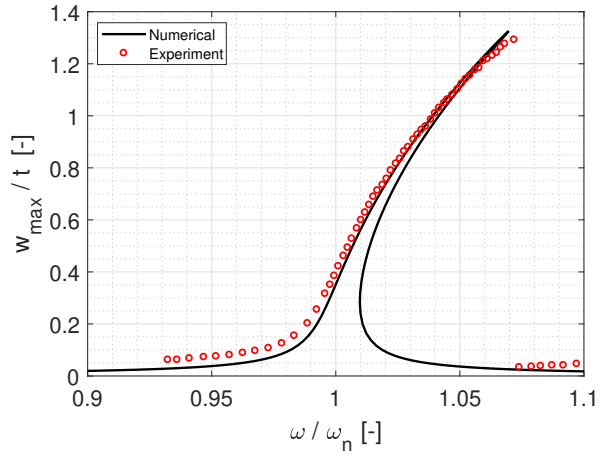

Figure 15: Comparison between experimental and numerical nonlinear frequency response curves of the stiffened plate when f=1.2N and is applied at x=0.2m, y=0.16m

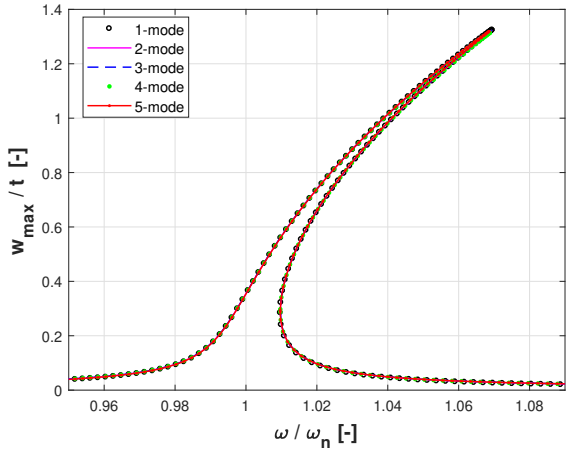

Figure 16: Comparison of frequency response curve at f=1.2N when the number of degrees of freedom in the ROM are varied from 1 to 5

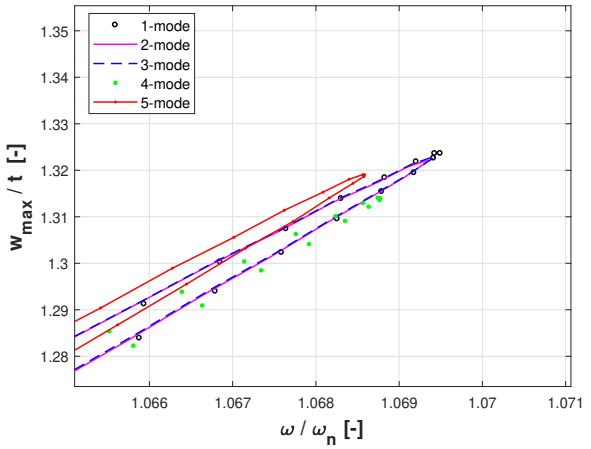

Figure 17: Comparison of frequency response curve at f=1.2N when the number of degrees of freedom in the ROM are varied from 1 to 5 - enlarged view at the tip of the curve

method applicable to nonlinear static stability problems and has been generated using a momentum subspace as the basis of transformation to the reduced system. A nonlinear mapping is assumed for the displacement variable to capture the effect of geometric nonlinearity. A single step computational procedure is required for the ROM formulation since the basis is purely dependent on the initial configuration of the structure. The ROM was initially tested by comparing the transient response of a rectangular plate subjected to dynamic loads with the results from Abaqus. Displacements and stress resultants have been computed for the plate and they have been found to be in excellent agreement with the results from Abaqus. Furthermore, the computations using the ROM was found to be at least thirty times faster than the full-scale FE model. The model reduction method has been tested further for a stiffened plate for which nonlinear modes were computed. A pseudo-arc length continuation algorithm has been used to solve the governing differential equations of the ROM for the stiffened plate. Frequency vs amplitude plots have been obtained for several load cases of forced vibration. Nonlinear vibration experiments were conducted using Polytec Laser Doppler Vibrometer and PAK MK-II systems to validate the ROM. The comparison of numerically computed peak nonlinear frequency in each

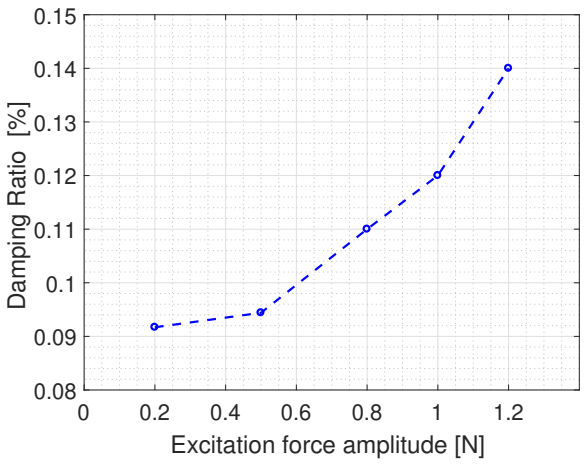

Figure 18: Variation in damping ratio with force amplitude

frequency response curve to the experimental peaks show a good agreement with a maximum deviation of only 0.38 %. Furthermore, accurate numerical results in comparison to the experimental data were achievable using only a single-degree of freedom ROM. Further considerations include incorporation of nonlinear damping models and application of the approach to large scale structural problems. Nevertheless, the formulation seems to show a good potential from our preliminary validation studies.

Acknowledgement

The authors would like to acknowledge the efforts of the staff in the Machining Laboratory of the Aerospace Structures and Materials department at Delft University of Technology, the Netherlands, in manufacturing the stiffened plate structure used for the experimental measurements. The authors would also like to acknowledge the support provided by the staff in Precision and Microsystems Laboratory of the Mechanical, Maritime and Materials Engineering department of Delft University of Technology, the Netherlands in conducting the experiments using Laser Vibrometer.

This research did not receive any specific grant from funding agencies in the public, commercial, or not-for-profit sectors.

References

References

[1] N. Morris, The use of modal superposition in nonlinear dynamics, Computers and Structures 7 (1977) 65–72. doi:10.1016/0045-7949(77)90061-X.

[2] E. Wilson, M.-W. Yuan, J. Dickens, Dynamic analysis by direct superposition of ritz vectors, Earthquake Engineering and Structural Dynamics 10 (1982) 813–821. doi:10.1002/eqe.4290100606.

[3] S. Rizzi, A. Przekop, Efficient modal basis selection criteria for efficient reduced order nonlinear simulation, Journal of Sound and Vibration 315 (2008) 467–485.

[4] B. Sajadi, S. Wahls, S. van Hemert, P. Belardinelli, P. G. Steeneken, F. Alijani, Nonlinear dynamic identification of graphene's elastic modulus via reduced order modeling of atomistic simulations, Journal of the Mechanics and Physics of Solids 122 (2019).

[5] B. Jacob, N. Ebecken, Adaptive reduced integration method for nonlinear structural dynamic analysis, Computers & structures 45 (1992) 333–347. doi:10.1016/0045-7949(92)90417-X.

[6] A. Noor, J. Peters, Reduced basis technique for nonlinear analysis of structures, AIAA Journal 18 (1980) 455–462.

[7] F. Alijani, M. Amabili, F. Bakhtiari-Nejad, On the accuracy of the multiple scales method for non-linear vibrations of doubly curved shallow shells, International Journal of Non-Linear Mechanics 46 (2011) 170–179. doi:10.1016/j.ijnonlinmec.2010.08.006.

[8] H. Chu, G. Herrmann, Influence of large amplitudes on free flexural vibrations of rectangular elastic plates, Journal of Applied Mechanics 23 (1956) 532–540.

[9] J. Eisley, Nonlinear vibrations of beams and rectangular plates, Journal of Applied Mathematics and Physics 15 (1964) 167–175.

[10] N. Yamaki, M. Chiba, Nonlinear vibrations of a clamped rectangular plate with initial deflection and initial edge displacement - part i: Theory, Thin Walled Structures 1 (1983) 3–29.
[11] N. Yamaki, K. Otomo, M. Chiba, Nonlinear vibrations of a clamped rectangular plate with initial deflection and initial edge displacement - part ii: Experiment, Thin Walled Structures 1 (1983) 101–119.
[12] A. Leung, S. Mao, A symplectic galerkin method for nonlinear vibrations of beams and plates, Journal of Sound and Vibration 183 (1995) 2587–2605. doi:10.1006/jsvi.1995.0266.
[13] W. Han, M. Petyt, Geometrically nonlinear vibration analysis of thin rectangular plates using the hierarchical finite element method - i: the fundamental mode of isotropic plates, Computers and Structures 63 (1997) 295–308.
[14] W. Han, M. Petyt, Geometrically nonlinear vibration analysis of thin rectangular plates using the hierarchical finite element method - ii: 1st mode of laminated plates and higher modes of isotropic and laminated plates, Computers and Structures 63 (1997) 309–318.
[15] F. Alijani, M. Amabili, Nonlinear vibrations of laminated and sandwich rectangular plates with free edges. part 1 : Theory and numerical simulations, Composite Structures 105 (2013) 422–436. doi:10.1016/j.compstruct.2013.05.034.
[16] M. Amabili, Reduced-order models for nonlinear vibrations, based on natural modes: the case of the circular cylindrical shell, Philosophical Transactions of the Royal Society A: Mathematical, Physical and Engineering Sciences 371 (2013).
[17] M. Amabili, M. Païdoussis, Review of studies on geometrically nonlinear vibrations and dynamics of circular cylindrical shells and panels, with and without fluid-structure interaction, Applied Mechanics 56 (2003) 349–381. doi:10.1115/1.1565084.
[18] F. Alijani, M. Amabili, Non-linear vibrations of shells: A literature review from 2003 to 2013, Applied Mechanics 58 (2014) 233–257. doi:10.1016/j.ijnonlinmec.2013.09.012.
[19] S. Idelsohn, A. Cardona, A reduction method for nonlinear structural dynamic analysis, Computer Methods in Applied Mechanics and Engineering 49 (1985) 253–279. doi:10.1016/0045-7825(85)90125-2.
[20] P. M. A. Slaats, J. de Jongh, A. A. H. J. Sauren, Model reduction tools for nonlinear structural dynamics, Computers & Structures 54 (1995) 1155–1171.
[21] W. Koiter, On the stability of the elastic equilibrium, Ph.D. thesis, Delft University of Technology, 1945.
[22] L. Rehfield, Nonlinear free vibrations of elastic structures, International Journal of Solids and Structures 9 (1973) 581–590. doi:10.1016/0020-7683(73)90071-1.
[23] P. Tiso, Finite element based reduction methods for static and dynamic analysis of thin-walled structures, Ph.D. thesis, TU Delft, Delft University of Technology, 2006.
[24] P. Tiso, Optimal second order reduction basis selection for nonlinear transient analysis, in: Modal Analysis Topics, Volume 3, Springer, 2011, pp. 27–39.
[25] C. S. Sombroek, P. Tiso, L. Renson, G. Kerschen, Numerical computation of nonlinear normal modes in a modal derivative subspace, Computers & Structures 195 (2018) 34–46.
[26] S. Jain, P. Tiso, J. B. Rutzmoser, D. J. Rixen, A quadratic manifold for model order reduction of nonlinear structural dynamics, Computers & Structures 188 (2017) 80–94.
[27] J. Rutzmoser, D. Rixen, P. Tiso, S. Jain, Generalization of quadratic manifolds for reduced order modeling of nonlinear structural dynamics, Computers & Structures 192 (2017) 196–209.
[28] K. Liang, A Koiter-Newton arclength method for buckling-sensitive structures, Ph.D. thesis, TU Delft, Delft University of Technology, 2013.
[29] K. Liang, M. Abdalla, Z. Gürdal, A Koiter-Newton approach for nonlinear structural analysis, International Journal for Numerical Methods in Engineering 96 (2013) 763–786.
[30] J. Argyris, An excursion into large rotations, Computer methods in applied mechanics and engineering 32 (1982) 85–155.
[31] H. Goldstein, C. Poole, J. Safko, Classical Mechanics, 3rd ed., Addison-Wesley, 2002.
[32] W. Greiner, Classical Mechanics: Systems of Particles and Hamiltonian Dynamics, Classical theoretical physics, Springer, 2009. URL: http://books.google.nl/books?id=NAo7yv7Jmq0C.
[33] K. Modin, G. Söderlind, Geometric integration of Hamiltonian systems perturbed by Rayleigh damping, BIT Numerical Mathematics 51 (2011) 977–1007.
[34] M. P. Mignolet, A. Przekop, S. A. Rizzi, S. M. Spottswood, Generalization of quadratic manifolds for reduced order modeling of nonlinear structural dynamics, Journal of Sound and Vibration 332 (2013) 2437–2460.
[35] C. Militello, C. Felippa, The first ANDES elements: 9-dof plate bending triangles, Computer methods in applied mechanics and engineering 93 (1991) 217–246. doi:10.1016/0045-7825(91)90152-V.
[36] K. Alvin, M. Horacio, B. Haugen, C. Felippa, Membrane triangles with corner drilling freedoms-I. The EFF element, Finite Elements in Analysis and Design 12 (1992) 163–187. doi:10.1016/0168-874X(92)90033-9.
[37] E. J. Doedel, Lecture notes on numerical analysis of nonlinear equation, in: B. Krauskopf, H. Osinga, J. Galán-Vioque (Eds.), Numerical Continuation Methods for Dynamical Systems, Springer, Dordrecht, 2007, pp. 1–49. doi:10.1007/978-1-4020-6356-5_1.
[38] M. Amabili, Nonlinear vibrations of rectangular plates with different boundary conditions: theory and experiments, Computers and Structures 82 (2004) 2587–2605. doi:10.1016/j.compstruc.2004.03.077.
[39] F. Alijani, M. Amabili, Theory and experiments for nonlinear vibrations of imperfect rectangular plates with free edges, Journal of Sound and Vibration 332 (2013) 3564–3588. doi:10.1016/j.jsv.2013.02.015.
[40] P. Balasubramanian, G. Ferrari, M. Amabili, Identification of the viscoelastic response and nonlinear damping of a rubber plate in nonlinear vibration regime, Mechanical Systems and Signal Processing 111 (2018) 376–398.
[41] M. Amabili, Nonlinear damping in nonlinear vibrations of rectangular plates: Derivation from viscoelasticity and experimental validation, Journal of the Mechanics and Physics of Solids 118 (2018) 275–292. doi:10.1016/j.jmps.2018.06.004.
[42] F. Alijani, M. Amabili, P. Balasubramanian, S. Carra, G. Ferrari, R. Garziera, Damping for large amplitude vibrations of plates and curved panels, part 1: Modelling and experiments, International Journal of Nonlinear Mechanics 85 (2016) 23–40. doi:10.1016/j.ijnonlinmec.2016.05.003.
[43] M. Amabili, F. Alijani, J. Delannoy, Damping for large-amplitude vibrations of plates and curved panels, part 2: Identification and comparisons, International Journal of Non-Linear Mechanics 85 (2016). doi:10.1016/j.ijnonlinmec.2016.05.004.

Appendix A. Derivation of conditions for a canonical transformation

This section contains the derivations for the conditions that ensure a canonical transformation. The derivation is initially performed using index notation, after which the matrix notation is introduced. The following transformation is adopted:

$$u_i = u_i(\boldsymbol{\xi}, \boldsymbol{\pi}) \tag{A.1a}$$

$$p_i = p_i(\boldsymbol{\xi}, \boldsymbol{\pi}). \tag{A.1b}$$

The derivatives $\dot{u}_i$ and $\dot{p}_i$ are computed:

$$\dot{u}_i = \frac{\partial u_i}{\partial \xi_j}\dot{\xi}_j + \frac{\partial u_i}{\partial \pi_j}\dot{\pi}_j \tag{A.2a}$$

$$\dot{p}_i = \frac{\partial p_i}{\partial \xi_l}\dot{\xi}_l + \frac{\partial p_i}{\partial \pi_l}\dot{\pi}_l, \tag{A.2b}$$

from which one can write:

$$\begin{aligned}
&\dot{p}_i \cdot \delta u_i - \dot{u}_i \cdot \delta p_i = \\
&\left(\frac{\partial p_i}{\partial \xi_l}\dot{\xi}_l + \frac{\partial p_i}{\partial \pi_l}\dot{\pi}_l\right) \cdot \left(\frac{\partial u_i}{\partial \xi_j}\delta\xi_j + \frac{\partial u_i}{\partial \pi_j}\delta\pi_j\right) - \\
&\left(\frac{\partial u_i}{\partial \xi_j}\dot{\xi}_j + \frac{\partial u_i}{\partial \pi_j}\dot{\pi}_j\right) \cdot \left(\frac{\partial p_i}{\partial \xi_l}\delta\xi_l + \frac{\partial p_i}{\partial \pi_l}\delta\pi_l\right).
\end{aligned} \tag{A.3}$$

Upon expanding the brackets the following form is obtained:

$$\begin{aligned}
&\dot{p}_i \cdot \delta u_i - \dot{u}_i \cdot \delta p_i = \\
&\frac{\partial p_i}{\partial \xi_l} \cdot \frac{\partial u_i}{\partial \xi_j}\dot{\xi}_l \cdot \delta\xi_j + \frac{\partial p_i}{\partial \xi_l} \cdot \frac{\partial u_i}{\partial \pi_j}\dot{\xi}_l \cdot \delta\pi_j + \\
&\frac{\partial p_i}{\partial \pi_l} \cdot \frac{\partial u_i}{\partial \xi_j}\dot{\pi}_l \cdot \delta\xi_j + \frac{\partial p_i}{\partial \pi_l} \cdot \frac{\partial u_i}{\partial \pi_j}\dot{\pi}_l \cdot \delta\pi_j - \\
&\frac{\partial u_i}{\partial \xi_j} \cdot \frac{\partial p_i}{\partial \xi_l}\dot{\xi}_j \cdot \delta\xi_l - \frac{\partial u_i}{\partial \xi_j} \cdot \frac{\partial p_i}{\partial \pi_l}\dot{\xi}_j \cdot \delta\pi_l - \\
&\frac{\partial u_i}{\partial \pi_j} \cdot \frac{\partial p_i}{\partial \xi_l}\dot{\pi}_j \cdot \delta\xi_l - \frac{\partial u_i}{\partial \pi_j} \cdot \frac{\partial p_i}{\partial \pi_l}\dot{\pi}_j \cdot \delta\pi_l
\end{aligned} \tag{A.4}$$

Terms are grouped:

$$\begin{aligned}
&\dot{p}_i \cdot \delta u_i - \dot{u}_i \cdot \delta p_i = \\
&\left(\frac{\partial p_i}{\partial \xi_l} \cdot \frac{\partial u_i}{\partial \xi_j} - \frac{\partial u_i}{\partial \xi_l} \cdot \frac{\partial p_i}{\partial \xi_j}\right) \cdot \dot{\xi}_l \cdot \delta\xi_j + \\
&\left(\frac{\partial p_i}{\partial \pi_l} \cdot \frac{\partial u_i}{\partial \pi_j} - \frac{\partial u_i}{\partial \pi_l} \cdot \frac{\partial p_i}{\partial \pi_j}\right) \cdot \dot{\pi}_l \cdot \delta\pi_j + \\
&\left(\frac{\partial u_i}{\partial \xi_l} \cdot \frac{\partial p_i}{\partial \pi_j} - \frac{\partial p_i}{\partial \xi_l} \cdot \frac{\partial u_i}{\partial \pi_j}\right) \\
&\cdot \left(\dot{\pi}_j \cdot \delta\xi_l - \dot{\xi}_l \cdot \delta\pi_j\right)
\end{aligned} \tag{A.5}$$

The following ordering for the matrix notation is introduced:

$$\frac{\partial \mathbf{p}}{\partial \boldsymbol{\xi}} = \begin{pmatrix} \frac{\partial p_1}{\partial \xi_1} & \frac{\partial p_1}{\partial \xi_2} & \cdots & \frac{\partial p_1}{\partial \xi_l} \\ \frac{\partial p_2}{\partial \xi_1} & \frac{\partial p_2}{\partial \xi_2} & \cdots & \frac{\partial p_2}{\partial \xi_l} \\ \vdots & \vdots & \ddots & \vdots \\ \frac{\partial p_i}{\partial \xi_1} & \frac{\partial p_i}{\partial \xi_2} & \cdots & \frac{\partial p_i}{\partial \xi_l} \end{pmatrix} \tag{A.6}$$

One can write:

$$
\begin{aligned}
&\dot{p}_i \cdot \delta u_i - \dot{u}_i \cdot \delta p_i = \\
&\left[\left(\frac{\partial \mathbf{p}}{\partial \boldsymbol{\xi}}\right)_{il} \cdot \left(\frac{\partial \mathbf{u}}{\partial \boldsymbol{\xi}}\right)_{ij} - \left(\frac{\partial \mathbf{u}}{\partial \boldsymbol{\xi}}\right)_{il} \cdot \left(\frac{\partial \mathbf{p}}{\partial \boldsymbol{\xi}}\right)_{ij}\right] \cdot \dot{\xi}_l \cdot \delta \xi_j + \\
&\left[\left(\frac{\partial \mathbf{p}}{\partial \boldsymbol{\pi}}\right)_{il} \cdot \left(\frac{\partial \mathbf{u}}{\partial \boldsymbol{\pi}}\right)_{ij} - \left(\frac{\partial \mathbf{u}}{\partial \boldsymbol{\pi}}\right)_{il} \cdot \left(\frac{\partial \mathbf{p}}{\partial \boldsymbol{\pi}}\right)_{ij}\right] \cdot \dot{\pi}_l \cdot \delta \pi_j + \\
&\left[\left(\frac{\partial \mathbf{u}}{\partial \boldsymbol{\xi}}\right)_{il} \cdot \left(\frac{\partial \mathbf{p}}{\partial \boldsymbol{\pi}}\right)_{ij} - \left(\frac{\partial \mathbf{p}}{\partial \boldsymbol{\xi}}\right)_{il} \cdot \left(\frac{\partial \mathbf{u}}{\partial \boldsymbol{\pi}}\right)_{ij}\right] \\
&\cdot \left(\dot{\pi}_j \cdot \delta \xi_l - \dot{\xi}_l \cdot \delta \pi_j\right).
\end{aligned}
\tag{A.7}
$$

In matrix form this is written as:

$$
\begin{aligned}
&\dot{\mathbf{p}}^t \delta \mathbf{u} - \dot{\mathbf{u}}^t \delta \mathbf{p} = \\
&\left[\left(\frac{\partial \mathbf{p}}{\partial \boldsymbol{\xi}}\right)^t \cdot \left(\frac{\partial \mathbf{u}}{\partial \boldsymbol{\xi}}\right) - \left(\frac{\partial \mathbf{u}}{\partial \boldsymbol{\xi}}\right)^t \cdot \left(\frac{\partial \mathbf{p}}{\partial \boldsymbol{\xi}}\right)\right] \cdot \dot{\boldsymbol{\xi}}^t \delta \boldsymbol{\xi} + \\
&\left[\left(\frac{\partial \mathbf{p}}{\partial \boldsymbol{\pi}}\right)^t \cdot \left(\frac{\partial \mathbf{u}}{\partial \boldsymbol{\pi}}\right) - \left(\frac{\partial \mathbf{u}}{\partial \boldsymbol{\pi}}\right)^t \cdot \left(\frac{\partial \mathbf{p}}{\partial \boldsymbol{\pi}}\right)\right] \cdot \dot{\boldsymbol{\pi}}^t \delta \boldsymbol{\pi} + \\
&\left[\left(\frac{\partial \mathbf{u}}{\partial \boldsymbol{\xi}}\right)^t \cdot \left(\frac{\partial \mathbf{p}}{\partial \boldsymbol{\pi}}\right) - \left(\frac{\partial \mathbf{p}}{\partial \boldsymbol{\xi}}\right)^t \cdot \left(\frac{\partial \mathbf{u}}{\partial \boldsymbol{\pi}}\right)\right] \\
&\cdot \left(\dot{\boldsymbol{\pi}}^t \delta \boldsymbol{\xi} - \dot{\boldsymbol{\xi}}^t \delta \boldsymbol{\pi}\right).
\end{aligned}
\tag{A.8}
$$

This yields the final conditions that ensure a canonical transformation, in matrix form:

$$\left[\left(\frac{\partial \mathbf{p}}{\partial \boldsymbol{\xi}}\right)^t \cdot \left(\frac{\partial \mathbf{u}}{\partial \boldsymbol{\xi}}\right) - \left(\frac{\partial \mathbf{u}}{\partial \boldsymbol{\xi}}\right)^t \cdot \left(\frac{\partial \mathbf{p}}{\partial \boldsymbol{\xi}}\right)\right] = \mathbf{0} \tag{A.9a}$$

$$\left[\left(\frac{\partial \mathbf{p}}{\partial \boldsymbol{\pi}}\right)^t \cdot \left(\frac{\partial \mathbf{u}}{\partial \boldsymbol{\pi}}\right) - \left(\frac{\partial \mathbf{u}}{\partial \boldsymbol{\pi}}\right)^t \cdot \left(\frac{\partial \mathbf{p}}{\partial \boldsymbol{\pi}}\right)\right] = \mathbf{0} \tag{A.9b}$$

$$\left[\left(\frac{\partial \mathbf{u}}{\partial \boldsymbol{\xi}}\right)^t \cdot \left(\frac{\partial \mathbf{p}}{\partial \boldsymbol{\pi}}\right) - \left(\frac{\partial \mathbf{p}}{\partial \boldsymbol{\xi}}\right)^t \cdot \left(\frac{\partial \mathbf{u}}{\partial \boldsymbol{\pi}}\right)\right] = \mathbf{I}. \tag{A.9c}$$

Appendix B. Finite element expressions

Appendix B.1. Geometric coordinates and element area

For the three-node triangular flat shell element the nodal geometric coordinates (x_1, y_1), (x_2, y_2), and (x_3, y_3) are defined as:

$$x_{ij} = x_i - x_j \tag{B.1}$$

$$y_{ij} = y_i - y_j, \tag{B.2}$$

with $i, j = 1, 2, 3$. Using these coordinates the element area is calculated from:

$$\mathcal{A} = \frac{y_{21} x_{13} - x_{21} y_{13}}{2}. \tag{B.3}$$

Appendix B.2. Linear strain-displacement matrix

The linear strain-displacement matrix B_l, is obtained from [36], and is defined by:

$$\mathsf{B}_l = \frac{1}{2\mathcal{A}} \begin{bmatrix} \mathsf{B}_1 & \mathsf{B}_2 & \mathsf{B}_3 \end{bmatrix}, \tag{B.4}$$

with

$$\mathsf{B}_1 = \begin{bmatrix} y_{23} & 0 & & \frac{y_{23}(y_{13}-y_{21})}{6} \\ 0 & x_{23} & [\mathbf{0}]_{3\times 3} & \frac{x_{32}(x_{32}-x_{12})}{6} \\ x_{32} & y_{23} & & \frac{x_{31}y_{13}-x_{12}y_{21}}{3} \end{bmatrix} \tag{B.5}$$

$$\mathsf{B}_2 = \begin{bmatrix} y_{31} & 0 & & \frac{y_{31}(y_{21}-y_{32})}{6} \\ 0 & x_{13} & [\mathbf{0}]_{3\times 3} & \frac{x_{13}(x_{12}-x_{23})}{6} \\ x_{13} & y_{31} & & \frac{x_{12}y_{21}-x_{23}y_{32}}{3} \end{bmatrix} \tag{B.6}$$

$$\mathsf{B}_3 = \begin{bmatrix} y_{12} & 0 & & \frac{y_{12}(y_{32}-y_{13})}{6} \\ 0 & x_{21} & [\mathbf{0}]_{3\times 3} & \frac{x_{21}(x_{23}-x_{31})}{6} \\ x_{21} & y_{12} & & \frac{x_{23}y_{32}-x_{31}y_{13}}{3} \end{bmatrix}. \tag{B.7}$$

Appendix B.3. Isoparametric coordinates

The triangular coordinates system is introduced for which holds [23]:

$$\zeta_1 + \zeta_2 + \zeta_3 = 1. \tag{B.8}$$

The relation between the Cartesian coordinate system and the isoparametric coordinates is given by:

$$\begin{bmatrix} 1 \\ x \\ y \end{bmatrix} = \begin{bmatrix} 1 & 1 & 1 \\ x_1 & x_2 & x_3 \\ y_1 & y_2 & y_3 \end{bmatrix} \begin{bmatrix} \zeta_1 \\ \zeta_2 \\ \zeta_3 \end{bmatrix}. \tag{B.9}$$

The relation between the partial derivatives in the Cartesian coordinate system and the isoparametric coordinate system then becomes:

$$\begin{bmatrix} \frac{\partial}{\partial x} \\ \frac{\partial}{\partial y} \end{bmatrix} = \begin{bmatrix} \mathbf{T}_x \\ \mathbf{T}_y \end{bmatrix} \begin{bmatrix} \frac{\partial}{\partial \zeta_1} \\ \frac{\partial}{\partial \zeta_2} \\ \frac{\partial}{\partial \zeta_3} \end{bmatrix}, \tag{B.10}$$

in which:

$$\mathbf{T}_x = \frac{1}{2\mathcal{A}} \begin{bmatrix} y_{23} & y_{31} & y_{12} \end{bmatrix} \tag{B.11}$$

$$\mathbf{T}_y = \frac{1}{2\mathcal{A}} \begin{bmatrix} x_{32} & x_{13} & x_{21} \end{bmatrix}. \tag{B.12}$$

Appendix B.4. Shape functions

The displacements components u, v and w are interpolated using linear shape functions given as [23]:

$$\begin{bmatrix} u \\ v \\ w \end{bmatrix} = \begin{bmatrix} \zeta_1 & 0 & 0 & & & \zeta_2 & 0 & 0 \\ 0 & \zeta_1 & 0 & [\mathbf{0}]_{3\times 3} & & 0 & \zeta_2 & 0 \\ 0 & 0 & \zeta_1 & & & 0 & 0 & \zeta_2 \\ & & & \zeta_3 & 0 & 0 & & \\ & [\mathbf{0}]_{3\times 3} & & 0 & \zeta_3 & 0 & [\mathbf{0}]_{3\times 3} & \\ & & & 0 & 0 & \zeta_3 & & \end{bmatrix} \mathbf{q}. \tag{B.13}$$

Appendix B.5. Constant matrices

The constant matrices K_{xx}, ,K_{yy} and K_{xy} used to form the B_{nl}, are defined as [23]:

$$\mathsf{K}_{xx} = \mathbf{B}_w^t \mathbf{T}_x^t \mathbf{T}_x \mathbf{B}_w + \mathbf{B}_v^t \mathbf{T}_x^t \mathbf{T}_x \mathbf{B}_v \tag{B.14}$$

$$\mathsf{K}_{yy} = \mathbf{B}_w^t \mathbf{T}_y^t \mathbf{T}_y \mathbf{B}_w + \mathbf{B}_u^t \mathbf{T}_y^t \mathbf{T}_y \mathbf{B}_u \tag{B.15}$$

$$\mathsf{K}_{xy} = \mathbf{B}_w^t \left(\mathbf{T}_x^t \mathbf{T}_y + \mathbf{T}_y^t \mathbf{T}_x \right) \mathbf{B}_w, \tag{B.16}$$

with:

$$\left[\mathbf{B}_w\right] = \begin{bmatrix} 0 & 0 & 1 & 0 & 0 & 0 & 0 & 0 & 0 \\ 0 & 0 & 0 & 0 & 0 & 0 & 0 & 0 & 1 \\ 0 & 0 & 0 & 0 & 0 & 0 & 0 & 0 & 0 \\ 0 & 0 & 0 & 0 & 0 & 0 & 0 & 0 & 0 \\ 0 & 0 & 0 & 0 & 0 & 0 & 0 & 0 & 0 \\ 0 & 0 & 0 & 0 & 0 & 1 & 0 & 0 & 0 \end{bmatrix} \tag{B.17}$$

$$\left[\mathbf{B}_u\right] = \begin{bmatrix} 1 & 0 & 0 & 0 & 0 & 0 & 0 & 0 & 0 \\ 0 & 0 & 0 & 0 & 0 & 0 & 1 & 0 & 0 \\ 0 & 0 & 0 & 0 & 0 & 0 & 0 & 0 & 0 \\ 0 & 0 & 0 & 0 & 0 & 0 & 0 & 0 & 0 \\ 0 & 0 & 0 & 0 & 0 & 0 & 0 & 0 & 0 \\ 0 & 0 & 0 & 1 & 0 & 0 & 0 & 0 & 0 \end{bmatrix} \tag{B.18}$$

$$\left[\mathbf{B}_v\right] = \begin{bmatrix} 0 & 1 & 0 & 0 & 0 & 0 & 0 & 0 & 0 \\ 0 & 0 & 0 & 0 & 0 & 0 & 0 & 1 & 0 \\ 0 & 0 & 0 & 0 & 0 & 0 & 0 & 0 & 0 \\ 0 & 0 & 0 & 0 & 0 & 0 & 0 & 0 & 0 \\ 0 & 0 & 0 & 0 & 0 & 0 & 0 & 0 & 0 \\ 0 & 0 & 0 & 0 & 1 & 0 & 0 & 0 & 0 \end{bmatrix}. \tag{B.19}$$